Volume 1 | Number 1 | Jan 2013 | Pages 1–100

PCCP

Physical Chemistry Chemical Physics
www.rsc.org/pccp

ROYAL SOCIETY OF CHEMISTRY

ROYAL SOCIETY OF CHEMISTRY

www.rsc.org/pccp

Influence of non-covalent modification of multiwalled carbon nanotubes on the crystallization behaviour of binary blend of polypropylene and polyamide6

Nabaneeta Mukhopadhyay, Ajay S. Panwar, Gulshan Kumar, I. Samajdar and Arup R.Bhattacharyya*

Department of Metallurgical Engineering and Materials Science, Indian Institute of Technology Bombay, Powai, Mumbai 400076, India

Abstract

Blends of polypropylene (PP) and polyamide 6 (PA6) with multiwalled carbon nanotubes (MWNTs) were prepared using different processing strategies in a twin-screw micro-compounder. The effect of MWNTs on the crystallization behaviour of the PP phase and the PA6 phase of the blend has been investigated through non-isothermal crystallization studies by differential scanning calorimetric analysis. Further, the effect of the addition of the compatibilizer (PP-g-MA) and the modification of MWNTs (m-MWNTs) with a non-covalent organic modifier (Li-salt of 6 amino hexanoic acid, Li-AHA), has also been studied in context to the crystallization behaviour of the PP and PA6 phase in the blend. The crystallization studies have indicated a significant increase in bulk crystallization temperature of PP phase in the blend in the presence of MWNTs. Moreover, the formation of 'trans-lamellar crystalline' structure consisting of PA6 'trans-crystalline lamellae' on MWNTs surface was facilitated in case blends prepared via 'protocol 2' as compared to the corresponding blends prepared via 'protocol 1'. Wide angle X-ray diffraction analysis has showed the existence of β-polymorph of the PP phase due to incorporation of the PA6 phase in the blend. Addition of MWNTs in the blends has facilitated further β-crystalline structure formation of the PP phase. In the presence of m-MWNTs, higher β-fraction was observed in the PP phase as compared to blend with pristine MWNTs. Addition of PP-g-MA has suppressed the β-phase formation in the PP phase in the

blend. X-ray bulk texture analysis revealed that incorporation of PA6 as well as pristine/modified MWNTs has influenced the extent of orientation of the PP chains towards specific crystalline plane in various blend compositions of PP and PA6.

Keywords: PP/PA6 blend, crystallization, MWNTs, WAXD, X-ray bulk texture

[*] Author to whom all the correspondence should be addressed:

E-mail: arupranjan@iitb.ac.in, Tel. No.: +91-22-2576-7634, Fax: +91-22-2572 6975

2

Introduction

Blend of polypropylene (PP) and polyamide 6 (PA6) is a well investigated polymer blend system by several research groups [1-10]. It has been observed that PA6 acts as a hetero-nucleating agent during non-isothermal crystallization of isotactic polypropylene (i-PP) [3, 5–8, 10–13]. This has manifested in a shift in bulk crystallization temperature (T_c) of PP to a higher temperature in the presence of PA6 phase [8, 10]. It has also been found that PP melt could form 'trans-crystalline' structure on the surface of the dispersed PA6 chains [17, 10], which also suggests the hetero-nucleating action of the PA6 phase. Various compatibilizers could be utilized to achieve a finer morphology of PP/PA6 blend. PP grafted maleic anhydride (PP-g-MA) is one of the most widely used compatibilizers reported for PP/PA6 blend system [2-6, 14–17], which acts as a reactive compatibilizer and leads to a finer domain size and narrower domain size distribution of the dispersed phase.

Besides compatibilizer, incorporation of any solid filler such as carbon nanotubes (CNTs) may also influence the morphology of the binary blend, which otherwise affects the crystallization behaviour of various semi-crystalline polymer matrices in the blends. Even, 'agglomerated' dispersion of CNTs could impart hetero-nucleating effect on semi-crystalline polymers. [18]. Various polymorphic 'trans-crystalline' structures of PP could be generated in the presence of CNTs depending on the method of preparation of PP/CNTs composites [19]. i-PP exhibits three different polymorphs, viz., α, β and γ-crystalline structure [20–21]. Amongst these, the monoclinic α-crystalline form is the most predominant crystalline form found in general. However, use of a β-nucleating agent or controlled shear stress can favour the occurrence of the hexagonal β phase [20–22]. The triclinic γ-form has a very minor occurrence [20-21].

Different polymorphs of PP could be achieved by introducing a semi-crystalline polymer to the PP matrix as well. However, the ability of the hetero-nucleating action of the semi-crystalline polymer plays a very important role on the occurrence of different polymorphs of PP [10, 23-24]. It has been observed that semi-crystalline polymer viz., poly (vinylidenefluoride); PVDF has a strong α-nucleating effect on PP, which may hinder the formation of the β-phase even at very low concentration [10, 24]. In the presence of PA6, α phase of i-PP is predominant even when a β-nucleating agent has been added to i-PP [10, 24]. PA6 has a moderate α-nucleating ability, so 'trans-crystalline' structure formation occurs only occasionally on PA6 droplets and individual β-spherulites may also form in the PP melt [10].

It has been observed that the incorporation of multiwalled carbon nanotubes (MWNTs) in the binary PP/PA6 blend leads to finer morphology irrespective of the type of phase morphology [25]. However, 'agglomerated' dispersion of MWNTs in the respective phases could be reduced significantly by the use of a non-covalent organic modifier [26, 27]. In addition, the use of a reactive compatibilizer is also necessary to establish interfacial interaction between the polymeric phases [28]. In view of this, it has been planned to investigate the effect of pristine as well modified MWNTs on the crystallization behaviour of PP as well as PA6 phase in binary blends of PP and PA6. Further, the effect of the incorporation of a reactive compatibilizer has also been investigated on the crystallization behaviour of PP and PA6 phase in the PP/PA6 blend in the presence of either pristine/modified MWNTs. Moreover, variation in processing protocol during melt-mixing has been studied in context to the crystallization behavior of PP and PA6 phase in the blend with MWNTs.

Experimental

Materials

Polypropylene (PP) was obtained from Reliance Industries Limited, Mumbai, India (H200MA) with a melt flow index of 23 (2.16 kg load, 190 °C). Polyamide 6 (PA6, zero-shear viscosity ~ 180 Pa.s at 260 °C) was obtained from GSFC, Gujarat, India (Gujlon M28RC, relative viscosity 2.8, M_v is 38,642 in 85% formic acid). Pristine multiwalled carbon nanotubes (MWNTs; NC 3100, average length: 1.5 µm, average diameter: 9.5 nm, carbon purity 95% as per manufacturer specifications; average diameter of ~ 9 nm from TEM measurement, I_d/I_g= 0.8 from Raman spectroscopic analysis) were obtained from Nanocyl SA, Belgium. Polypropylene grafted maleic anhydride (PP-g-MA) of density 0.91 g/ml and maleic anhydride content (MAH) ranges from 1.6-2.5% having MFI value of 40 (P-408) was procured from Pluss Polymers, Haryana, India. 6 Amino hexanoic acid (AHA) (Sigma Aldrich, M_w = 132.18; purity: 98%) was neutralized using lithium hydroxide (Sisco Research Laboratories, India, purity: 98%) to obtain lithium salt of AHA (Li-AHA). The detailed procedure to obtain Li-AHA and the solid mixture of MWNTs and Li-AHA is described in the subsequent section.

Modification of MWNTs

Li-AHA was prepared by reacting 6-amino hexanoic acid with lithium hydroxide in deionized water (DI water) at~80-90 °C. The modification procedure is described below:

Initially, MWNTs were taken in DI water and sonicated in a bath ultra-sonicator (Vibronics, India, frequency 20 KHz) for 10 min. Then appropriate amount of Li-AHA was then dissolved in DI water and the solution was added to MWNTs dispersion and then sonicated for another 10 min. Subsequently, water was evaporated by heating; MWNTs/Li-AHA mixture (1:1, wt/wt) was dried at ~ 100 °C in the vacuum oven for 24 h. Henceforth, 1:1 (wt/wt) solid mixture of Li-AHA modified MWNTs will be denoted as m-MWNTs.

Sample Preparation

PP/PA6 blends with 5 wt% of pristine and m-MWNTs were prepared by melt-mixing in a conical twin-screw micro-compounder (Micro 5, DSM Research, Netherlands) at 260 °C with a rotational speed of 150 rpm (Please see Table 1 for detail blend composition). In the sequential mixing protocol, PP with 5 wt% pristine/m-MWNTs were initially mixed for 10 min followed by the addition of PA6 and melt-mixed for another 5 min (under the same extrusion conditions mentioned above, hereafter termed as 'PP based sequence' or 'protocol 1'). Similarly, PA6 with 5 wt% pristine or m-MWNTs were melt-mixed for 10 min followed by the addition of PP and melt-mixed for another 5 min (hereafter termed as 'PA6 based sequence' or 'protocol 2'). In case of blend with compatibilizer (PP-g-MA), compatibilizer has always been added to the PP phase and the same protocol as above was followed. All the experiments were performed under nitrogen atmosphere to prevent any oxidative degradation.

Injection-molded samples (according to ASTM D 638, Type V) were prepared using mini injection-moulding machine from DSM Research, Netherlands. The following protocols were utilized during the sample preparation of injection-moulding: injection pressure of 3 bar, melt temperature of 260 °C, mould temperature of 60 °C, holding time of 60 sec, and cooling time of 2–3 min. The sample codes of the corresponding blend compositions are shown in Table 1.

Characterizations

Transmission electron microscopic analysis was performed on a JEOL JEM-2100 F (Japan) microscope at 200 kV. Pristine MWNTs and m-MWNTs were dispersed in de-ionized water. Further, a drop of this dispersion was placed on the grid and dried to remove the solvent. For the composite samples, extrudate strands were ultra-micromed to prepare ~60 nm slice using Leica

ultra-microtome and finally the sample was collected on a 200 mesh copper grids covered with thin amorphous carbon film. Further, the sample was stained with ruthenium tetroxide (RuO_4) vapour for 1 hour to stain the PA6 phase.

Raman spectroscopy was performed using a HR 800 micro-Raman (Jobin Yovon, France) on powder samples over a scanning range of 1000-2000 cm^{-1} with incident laser excitation wavelength of 514 nm.

Brunauer-Emmet and Teller analysis (BET) was carried out by nitrogen adsorption method using surface area analyzer (Smart Instruments, Thane, India).

Differential scanning calorimetric (DSC) measurements were carried out using a modulated DSC (Q200 from TA Instruments, USA). The extrudate samples of about 4-5 mg were dried in a vacuum oven prior to experiment. The 'heating-cooling-heating' cycles were recorded in the temperature range from -50 °C to 260 °C at the scan rate of ±10 °C/min under nitrogen atmosphere. In the first heating run, all the samples were annealed at the final temperature (260 °C) for 3-4 min to delete the previous thermal history.

Morphology of PP/PA6 blends was studied through scanning electron microscopic analysis (SEM) using a Hitachi (S3400N, Japan) instrument. Extrudate strands were cryofractured in liquid nitrogen and then selectively etched (formic acid for PA6 phase). The etched surface was gold sputtered to avoid the charging of the sample.

Wide angle X-ray diffraction (WAXD) analysis was carried out on a Philips X-Pert Pro. The incident X-rays (λ=1.54 Å) from the Cu-target was monochromatized using a Ni filter. XRD patterns were recorded with a step scan with step size of 0.02 between 2θ =5°-50°.

A PANalytical MRD system was used in order to carry out bulk texture analysis. A relatively large area scan (2 mm X 2mm) was used for the XRD measurements to maintain reasonable statistics. Four pole figures were measured for bulk crystallographic texture. Subsequent texture analyses were conducted through a commercial program LaboTex [29]. Pole figures [30] were used for texture representation.

Results and Discussion

a. Characterization of pristine and m-MWNTs

Pristine and non-covalently modified MWNTs (m-MWNTs) were characterized using transmission electron microscopy (TEM), Raman spectroscopy and Brunauer-Emmet and Teller analysis (BET). Fig.1 shows TEM micrographs of pristine and m-MWNTs. MWNTs exhibit debundled and well dispersed after the modification, whereas pristine MWNTs show entangled network. The average diameter of MWNTs is increased from ~9.04 nm to ~9.59 nm due to the adsorption of Li-AHA molecules on the surface of MWNTs by the organic modifier. The I_d/I_g ratio corresponding to pristine MWNTs and m-MWNTs were calculated using Raman spectroscopic analysis. I_d/I_g ratio varies marginally on modification of MWNTs. Specific surface area of m-MWNTs reduces from 275 m^2/gm to 42.36 m^2/gm after Li-AHA modification. This suggests that the organic modifier adsorbs on the MWNTs surface.
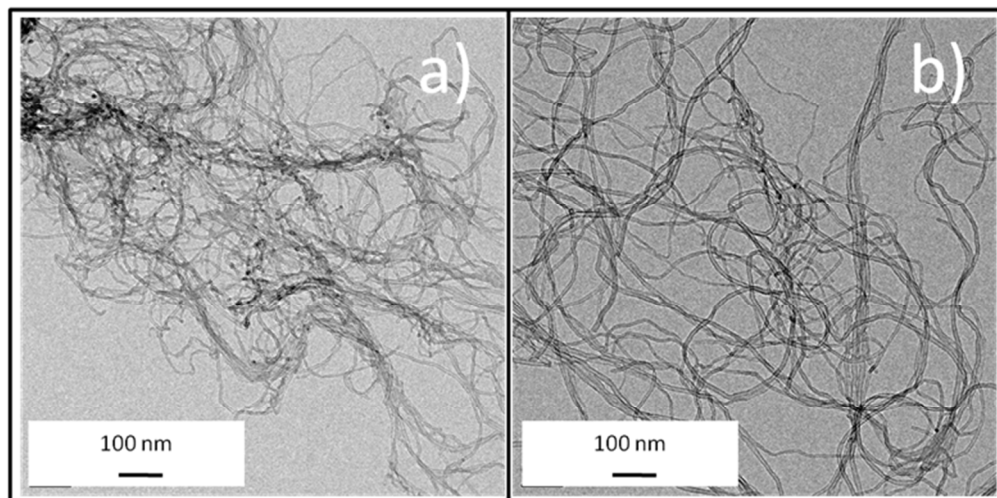
Figure 1: TEM micrographs of a) pristine MWNTs and b) m-MWNTs

b. Non-isothermal crystallization behaviour of PP and PA6 phase in PP/PA6 blends

Fig. 2 (a) shows the non-isothermal crystallization behavior of neat PP, PA6 and 40/60-60/40 (wt/wt) PP/PA6 blends. The bulk crystallization temperature (T_c) for PP is observed at ~115 °C and for PA6; T_c is shown at ~ 192 °C. In case of PP/PA6 blend, PP registers higher T_c at ~122 °C due to the hetero-nucleating action of the PA6 phase [3, 5–8, 10–13]. However, no significant change is observed in the T_c of the PA6 phase in the blend (Fig. 2a).
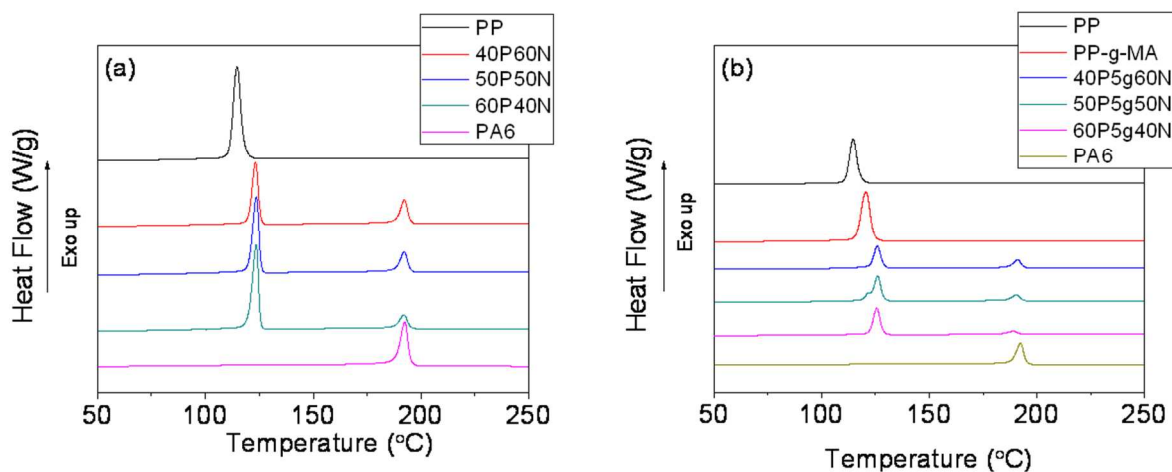
Figure 2: Crystallization exotherms of (a) neat PP, neat PA6 and PP, PA6 phase in the PP/PA6 blends; (b) neat PP, neat PA6, neat PP-g-MA and PP, PA6 phase in the PP/PA6 blends with 5 wt% PP-g-MA

Fig. 2 (b) exhibits the non-isothermal crystallization behavior of neat PP, PA6, PP-g-MA and 40/60-60/40 (wt/wt) PP/PA6 blends with 5 wt% PP-g-MA. Neat PP-g-MA depicts significantly higher T_c as compared to pure PP ($\sim$120.6 °C). In the presence of PP-g-MA, T_c corresponding to PP shifts to the higher temperature side ($\sim$125.8 °C) in the neat blend. Further, in case of 50/50 (wt/wt) PP/PA6 blend, PP phase exhibits a small peak at $\sim$121.5 °C along with the presence of another peak at $\sim$125.9 °C. Further, T_c corresponding to the PA6 phase gradually decreases with decreasing concentration of the PA6 phase in the blend in the presence of PP-g-MA. A similar behaviour was reported earlier by Moon et al., wherein T_c of the PA6 phase was decreased with increasing concentration of PP-g-MA due to the formation of the graft copolymer at the interface, which leads to a delay in the crystallization of the PA6 phase [3]. It has also been reported earlier that the presence of PP-g-PA6 could influence the crystallization behaviour of both PP and PA6 phase due to the finer morphology development or due to the alteration of the type of phase morphology [31].

c. Non-isothermal crystallization behaviour of PP/PA6 blends in the presence of MWNTs

In this section, the effect of MWNTs on the crystallization behaviour of PP as well as PA6 phase in various compositions of PP/PA6 blend is reported, wherein m-MWNTs were incorporated in the blends in the presence of PP-g-MA. Moreover, all these compositions were prepared either following 'protocol 1'or via 'protocol 2'. It is envisaged that the modification of MWNTs with Li-AHA leads to smaller 'agglomerates' of MWNTs along with 'individualized' MWNTs during melt-mixing [27]. Further, the addition of PP-g-MA may not only improve the interfacial interaction between the phases, but also interact with the Li-AHA modified MWNTs.

Moreover, the two sequences may also improve the interaction between the corresponding phase and MWNTs, thereby may retain a higher fraction of MWNTs in the respective phase. In view of this, it is necessary to understand the effect of the addition of the individual components in the neat blend as well. It is to be noted that the variation in T_c in the respective phase (PP as well as PA6 phase) in the blend with MWNTs has been considered as a signature for hetero-nucleating action during non-isothermal crystallization studies. Further, the effectiveness of the hetero-nucleating action of MWNTs may depend on the 'agglomerates' or 'individualized' MWNTs dispersion in the blend. Moreover, polymer wrapping (viz., in case of PA6 or due to melt-interfacial reaction in the presence of PP-g-MA) on MWNTs may eventually lower the extent of hetero-nucleating action of MWNTs.

Fig. 3 (a) depicts T_c of PP and PA6 phase in neat 50/50 (wt/wt) PP/PA6 blend and the corresponding blends in the presence of the organic modifier (Li-AHA), PP-g-MA and in the presence of both Li-AHA and PP-g-MA. It is observed that in the presence of Li-AHA, T_c of the PP phase exhibits a shift at higher temperature in 50/50 (wt/wt) PP/PA6 blend than neat PP but lower than neat PP/PA6 blend. The extent of hetero-nucleating action of the PA6 phase may be decreased due to the plasticization and/or chain scission of the PA6 phase in the presence of Li-AHA like molecule [32, 33]. Further, Li-AHA may also plasticize PP phase as well [28]. In the presence of the compatibilizer (PP-g-MA), PP phase shows an enhanced T_c as per our earlier observation. In the presence of both Li-AHA and PP-g-MA, the crystallization behaviour of the PP phase shows a similar behaviour as that of the corresponding blend without the addition of the compatibilizer, which suggests the dominant role of Li-AHA in delaying the rate of crystallization of the PP phase. On the other hand [Fig. 3 (b)], PA6 phase shows a decrease in the T_c irrespective of the compositional variation. Chain scission of the PA6 phase may occur in the

11

presence of Li-AHA, which may delay the rate of crystallization of the PA6 phase marginally. In addition, PP-g-MA may as well delay the rate of crystallization of the PA6 phase due to the melt-interfacial reaction, between maleic anhydride functionality of PP-g-MA and the amine end group of the PA6 phase.

Fig. 3 (c) and (d) show the morphology of the neat 50/50 (wt/wt) PP/PA6 blend and 50/50 (wt/wt) PP/PA6 blend with 5 wt% of Li-AHA. The morphology is partially co-continuous along with the presence of few PA6 droplets in 50/50 PP/PA6 blend. In the presence of Li-AHA [fig. 3 (d)], PA6 domains are appeared to be elongated and eventually form coarse co-continuous structure. The broad ligament thickness associated with the PA6 phase manifests the plasticization and/or chain scission phenomenon of the PA6 phase in the presence of Li-AHA. On the other hand, the addition of PP-g-MA leads to the change in the type of phase morphology, wherein PA6 phase forms finer droplets in the continuous PP phase [fig. 3(e)]. This indicates the compatibilization action of PP-g-MA in the blend. This type of behaviour was earlier reported by Ohlsson et al. and Roeder et al. in case of PA6 and styrene/ethylene-co-butylene/styrene grafted with maleic anhydride (SEBS-g-MA) [34, 35]. Fig. 3 (f) shows the morphology of 50/50 (wt/wt) PP/PA6 blend in the presence of Li-AHA and PP-g-MA. Fully developed co-continuous structure is observed, wherein plasticization and/or chain scission of the PA6 phase along with melt-interfacial reaction induced by PP-g-MA may tune the phase morphology. Moreover, the co-continuous morphology is finer as compared to the addition of Li-AHA incorporated neat blend.

Fig. 4 (a) exhibits the crystallization exotherms of the PP phase in PP/PA6 blend in the presence of pristine MWNTs prepared via 'protocol 1' and 'protocol 2'. In the presence of pristine MWNTs, PP phase shows an enhanced T_c irrespective of the processing protocol

suggesting the hetero-nucleating action of MWNTs. However, some of the blend compositions show a lesser extent of hetero-nucleating action of MWNTs. This may be due to the retention of a major fraction of MWNTs during melt-mixing in the PA6 phase due to the lower surface energy difference between PA6 and MWNTs. This observation has been manifested in lower T_c of the PP phase of the blends, which have been prepared via 'protocol 2' as compared to the PP phase of the corresponding blends prepared via 'protocol 1'. Further, some of the blend compositions also show a small crystallization peak at ~ 134 °C, which will be discussed later.

Fig. 4 (b) shows the crystallization exotherms of the PA6 phase in PP/PA6 blend with pristine MWNTs prepared via 'protocol 1' and 'protocol 2'. PA6 phase exhibits double exothermic crystallization peak on incorporation of pristine MWNTs. Crystallization peak observed at higher temperature is due to the 'trans-lamellar crystalline' structure of the PA6 phase induced by the 'individualized' MWNTs due to the lattice matching between PA6 and MWNTs. Such observations were earlier reported by Phang et al. [36] and Leibler et al. [37].The 'trans-lamellar crystalline' morphology manifests in higher T_c as compared to the bulk T_c of the PA6 phase, which also shows the hetero-nucleating action of the 'agglomerated' MWNTs [38]. The peak observed at lower temperature is due to the bulk crystallization of PA6 phase in the presence of 'agglomerated' MWNTs. No significant variation in the peak position is observed in the blend prepared via different processing protocol; however, variation in the intensity ratio of the crystallization peaks is observed in various compositions, which is analyzed in the subsequent section.

Fig. 4 (c) depicts the crystallization exotherms of the PP phase in PP/PA6 blend with m-MWNTs prepared via 'protocol 1' and 'protocol 2'. It is to be noted that the blend with m-MWNTs irrespective of their protocol of mixing sequence shows a decrease in T_c of the PP

phase as compared to blend with pristine MWNTs. A similar behaviour is also observed in neat blend in the presence of Li-AHA [Fig. 3 (a)]. Further, it is also observed that the PP phase of the blend prepared via 'protocol 2' exhibits a higher T_c as compared to the PP phase of the blend prepared via 'protocol 1' in the presence of m-MWNTs. This observation may be explained on the basis that a fraction of 'exfoliated' MWNTs might have migrated from the PA6 phase to the PP phase, hence might have increased the number of hetero-nucleating sites as compared to the blend with pristine MWNTs prepared via 'protocol 2'.

Fig. 4 (d) presents the crystallization exotherms of the PA6 phase in PP/PA6 blend with m-MWNTs prepared via 'protocol 1' and 'protocol 2'. PA6 phase exhibits double exothermic crystallization peak as discussed earlier. However, no significant change is observed in the peak position due to different mixing sequences and due to the variation in the blend composition.
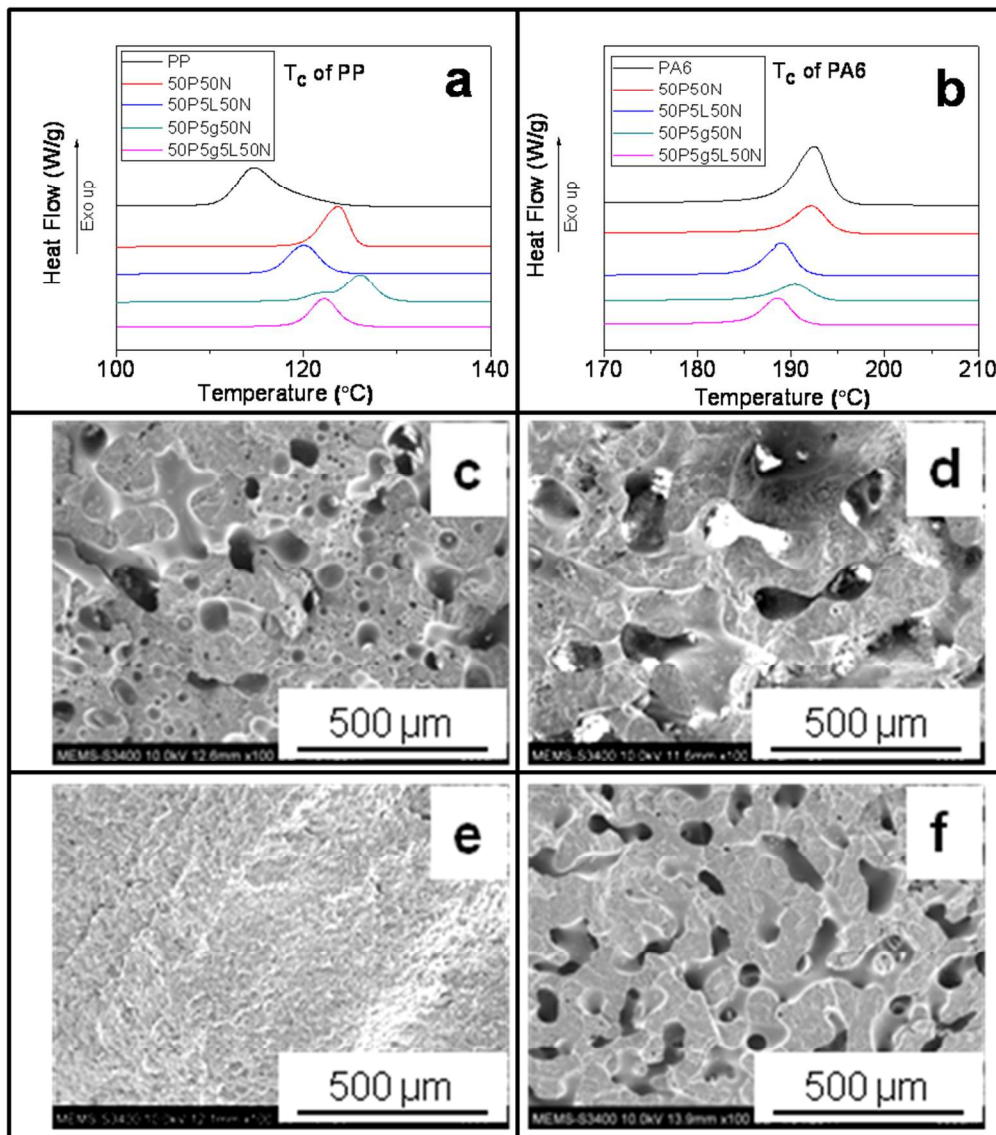
Figure 3: Crystallization exotherms of (a) PP and (b) PA6 phase in 50/50 (wt/wt) PP/PA6 blend with 5 wt% Li-AHA, 5 wt% PP-g-MA and (5+5) wt% of Li-AHA+PP-g-MA; SEM investigation of (c) neat 50/50 (wt/wt) PP/PA6 blend, (d) blend in the presence of Li-AHA, (e) blend in the presence of PP-g-MA, (f) blend in the presence of PP-g-MA and Li-AHA
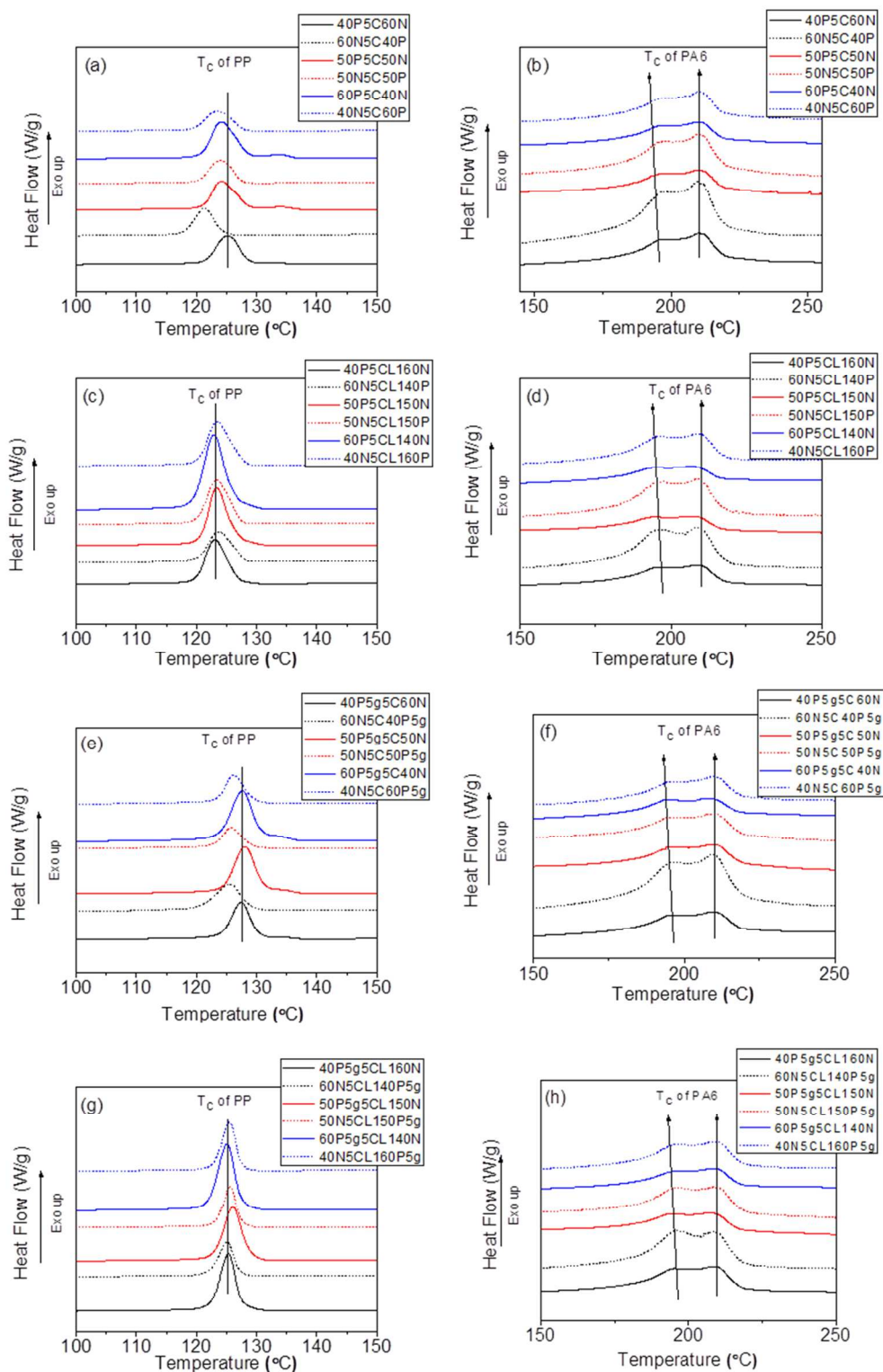
Figure 4: Crystallization exotherms of PP and PA6 phase in the PP/PA6 blend with (a, b) pristine MWNTs, (c, d) m-MWNTs,(e, f) PP-g-MA and pristine MWNTs, (g, h) PP-g-MA and m-MWNTs

Fig. 4 (e) and (g) exhibit the crystallization exotherms of the PP phase in PP/PA6 blend with pristine as well as with m-MWNTs in the presence of PP-g-MA prepared via 'protocol 1' and 'protocol 2'. In the presence of PP-g-MA, blend with pristine as well as m-MWNTs show higher T_c of the PP phase as compared to the corresponding uncompatibilized blend. This observation may be explained on the basis of the compatibilization action of PP-g-MA, which may not allow a majority fraction of MWNTs to migrate to the PA6 phase during melt-mixing. Further, blend prepared via 'protocol 1'shows a higher T_c of the PP phase as compared to the blend prepared via 'protocol 2' in the presence of pristine MWNTs and PP-g-MA, which may be explained on the basis that Li-AHA may engage in reacting with PP-g-MA, hence, a majority fraction of m-MWNTs migrating to the PP phase could be prevented. Moreover, in case of blend with PP-g-MA and pristine MWNTs, a shoulder near the first crystallization peak is observed. This peak is also observed in case of uncompatibilized blends with pristine MWNTs [Fig. 4 (a)]. This may be due to the fractionated crystallization of the PA6 droplets, which earlier has been observed in case of partially co-continuous morphology and 'matrix dispersed-droplet' morphology [3, 7, 39-41]. In the presence of pristine MWNTs, partially co-continuous morphology along with sub-inclusions of PA6 droplets has been observed [Fig. not shown here]. In the presence of a compatibilizer, this effect can be more prominent as the average droplet size of the PA6 phase may decrease significantly, which cannot crystallize at the bulk crystallization temperature [Fig. not shown here]. In the presence of m-MWNTs (for both uncompatibilized and compatibilized), this peak is not observed. Moreover, in the presence of m-MWNTs, well developed co-continuous morphology is observed as compared to the blends with pristine MWNTs. Hence, fractionated crystallization of PA6 could not occur due to unavailability of the PA6 phase as sub-micron size droplets. In the presence of m-MWNTs, blend prepared via 'protocol 2' shows

17

higher T_c of the PP phase as compared to the blend prepared via 'protocol 1', which is similar to Fig. 4 (c).

Fig. 4 (f) and (h) show the crystallization exotherms of the PA6 phase in PP/PA6 blend with pristine and m-MWNTs in the presence of PP-g-MA prepared via 'protocol 1' and 'protocol 2'. In the presence of PP-g-MA, blend with pristine MWNTs shows a decrease in both T_{c1} and T_{c2} corresponding to the PA6 phase in the blend prepared via 'protocol 1'as compared to corresponding uncompatibilized blend. However, T_{c1} corresponding to the PA6 phase increases in the blend with PP-g-MA and pristine MWNTs in case of blend prepared via 'protocol 2'. In the presence of PP-g-MA, blend with m- MWNTs does not exhibit any significant change in T_{c1} and T_{c2} corresponding to the PA6 phase as compared to the corresponding uncompatibilized blend. The above observation may be rationalized by the fact that the extent of melt-interfacial reaction would be different due to the different protocol of mixing and also due to the different extent of reaction between Li-AHA and PP-g-MA and/or PA6 phase.
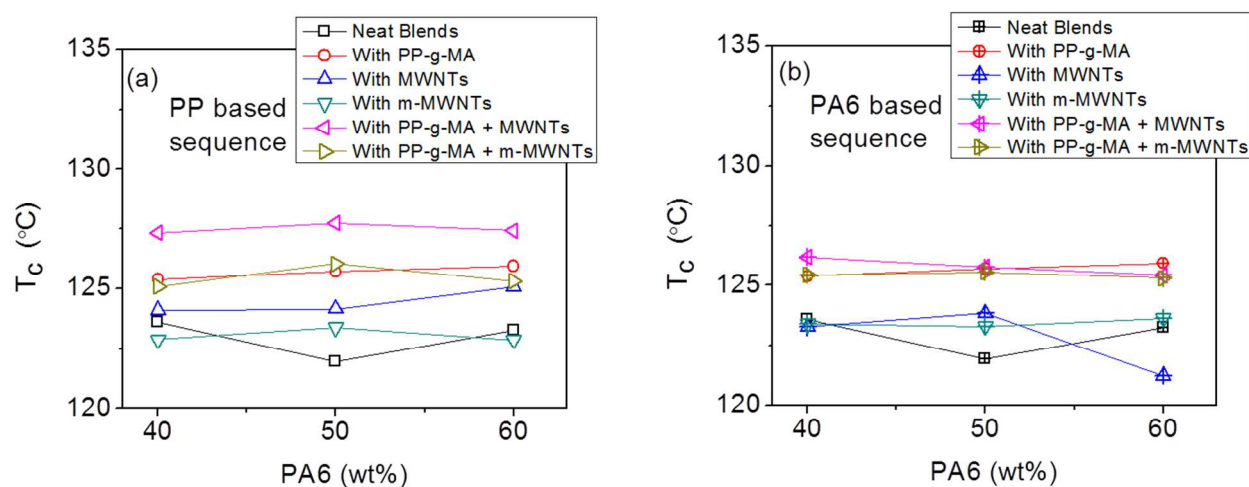

Figure 4: Crystallization temperature of the PP phase with increasing concentration of the PA6 phase in the blends prepared via 'protocol 1' and protocol 2'

Fig. 4 shows the variation in the crystallization temperature of the PP phase with increasing concentration of the PA6 phase in the blend, wherein the individual effect of PP-g-MA, pristine MWNTs, m-MWNTS, pristine MWNTs and m-MWNTs in the presence of PP-g-MA has been studied for the blends prepared via 'protocol 1' and 'protocol 2'. It is observed that T_c of the PP phase is almost independent of the blend composition. However, the effect of the individual component is quite significant. The compatibilized blend shows much higher T_c as compared to uncompatibilized neat blend. However, for other cases, effect of different sequences is not that significant.
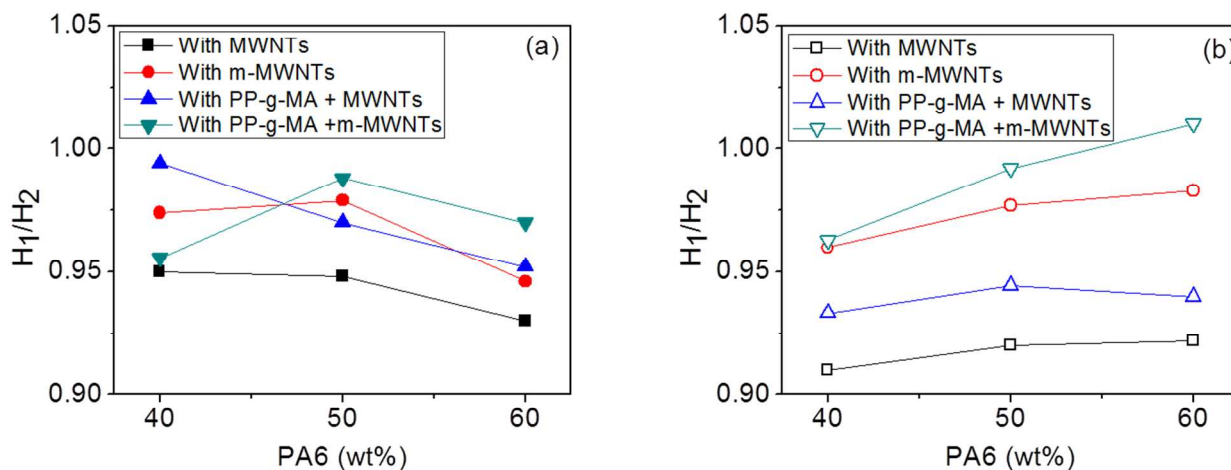

Figure 5: Crystallization peak intensity ratio (H_1/H_2) of the PA6 phase with increasing concentration of the PA6 phase in the blend prepared via (a) 'protocol 1'and (b) 'protocol 2'

Fig. 5 shows the crystallization peak intensity ratio (H_1/H_2) of the PA6 phase with increasing concentration of the PA6 phase in case of blends prepared via 'protocol 1' and 'protocol 2'. The effect of addition of pristine and m-MWNTs has been studied in the presence and absence of PP-g-MA. In all the cases, blends prepared via 'protocol 1' show a decrease of H_1/H_2 value with increasing concentration of the PA6 phase in the blend, however in case of blends prepared via 'protocol 2', the corresponding ratio increases with increasing concentration

of the PA6 phase in the corresponding blends. This may be due to the fact that 'trans-lamellar crystalline' structure formation is favoured in case of blends prepared via 'protocol 2', wherein MWNTs were initially mixed with the PA6 phase. The 'trans-crystalline' structure formation of the PA6 phase in the presence of MWNTs has earlier been reported by Leibler et al. [37]. 40/60 (wt/wt) PP/PA6 blend with pristine MWNTs prepared via 'protocol 2' shows the lowest value of H_1/H_2 ratio. The corresponding blend with m-MWNTs (in the presence and the absence of PP-g-MA) shows higher value of H_1/H_2. This may be due to the crystal lattice matching between PA6 and MWNTs where the PA6 chains stack perpendicularly to the individualized MWNTs surface, with the polyamide chains parallel to the axis of the MWNTs [37]. This observation also suggests the localization of higher fraction of 'individualized' MWNTs in the 40/60 (wt/wt) PP/PA6 blend. In the presence of m-MWNTs, Li-AHA molecules, which adsorbed on the surface of MWNTs, might engage in the melt-interfacial reaction between PA6 chains and the amine group of Li-AHA. In the presence of PP-g-MA, higher fraction of PA6 chains may also interact with the maleic anhydride functionality of PP-g-MA, which may hinder the induction of 'trans-crystalline lamellar' structure formation. Thus, the corresponding H_1/H_2 value might be higher in case of PP/PA6 blend with m- MWNTs (in the presence and absence of PP-g-MA) as compared to the corresponding blend with pristine MWNTs.

TEM investigation has been carried out for representative blend samples and it has been demonstrated that considerable amount of MWNTs are migrating from one phase to the other phase irrespective of the mixing sequence Fig. 6 depicts the TEM micrographs of 50/50 (wt/wt) PP/PA6 blends with pristine MWNTs prepared via (a) 'protocol 1' and (b) 'protocol 2'. PA6 phase has been stained using RuO_4. From the micrographs, it is evident that MWNTs could be observed in both the phases irrespective of the mixing protocol.
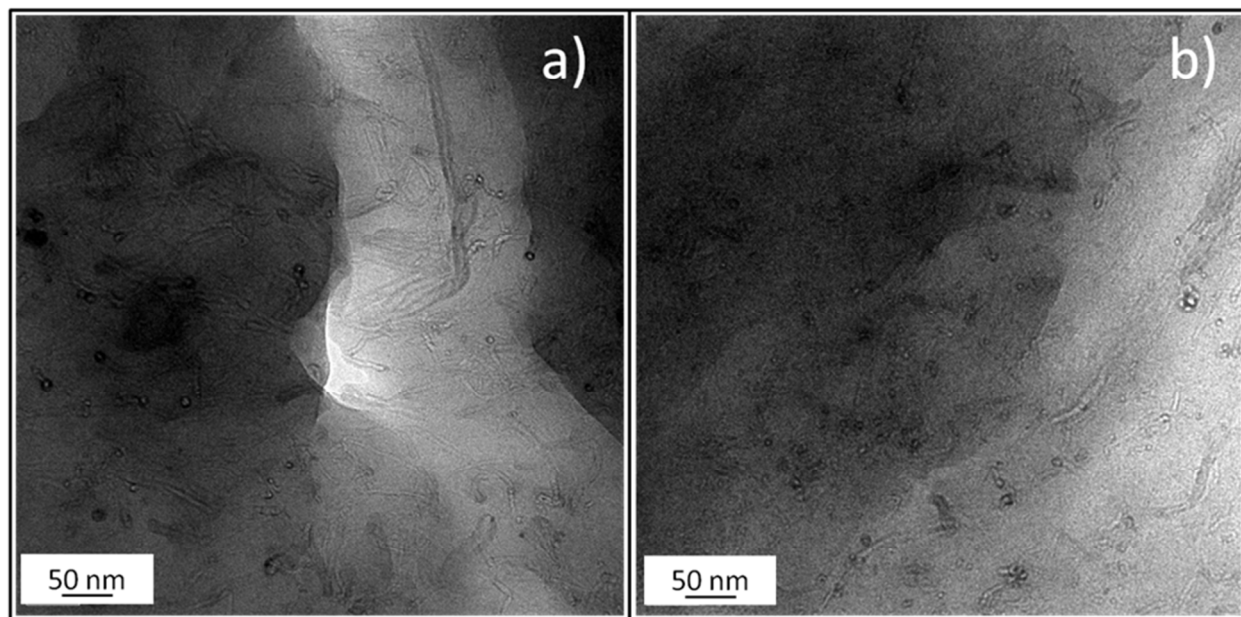
Figure 6: TEM micrographs of blends of 50/50 PP/PA6 (wt/wt) blend with 5 wt% MWNTs prepared via a) 'protocol 1' b) 'protocol 2' Full width at half maxima (FWHM) of PP crystallization exotherm was calculated to estimate the crystal size distribution of the PP phase as a function of blend composition. FWHM value of pure PP and the neat 50/50 blend of PP/PA6 are 4.04 °C and 3.2 °C respectively. Fig. 7 depicts the FWHM of PP with increasing content of the PA6 phase for the blends prepared via (a) 'protocol 1' and (b) 'protocol 2'. In case of PP/PA6 blends with pristine/m-MWNTs in the presence and in the absence of PP-g-MA, the distribution is almost independent of the blend compositions in most of the cases. However, blends with pristine MWNTs exhibit higher FWHM values as compared to other blend samples. This suggests smaller crystal size distribution in the presence of pristine MWNTs. Blends with m-MWNTs along with PP-g-MA exhibit highest crystal size distribution amongst all the blend samples. However, blends with only m-MWNTs and blends with pristine MWNTs along with PP-g-MA show intermediate values of FWHM of PP. A similar trend is observed in case of blends prepared via 'protocol 2' [Fig. 7 (b)]. However, blends with pristine MWNTs show an

increasing crystal size distribution with increasing content of the PA6 phase. Moreover, blends with pristine MWNTs along with PP-g-MA exhibit a decrease in the crystal size distribution with increasing content of the PA6 phase. Highest crystal size distribution is observed in case of blends with m-MWNTs along with PP-g-MA, which is similar to the blends prepared via 'protocol 1'.
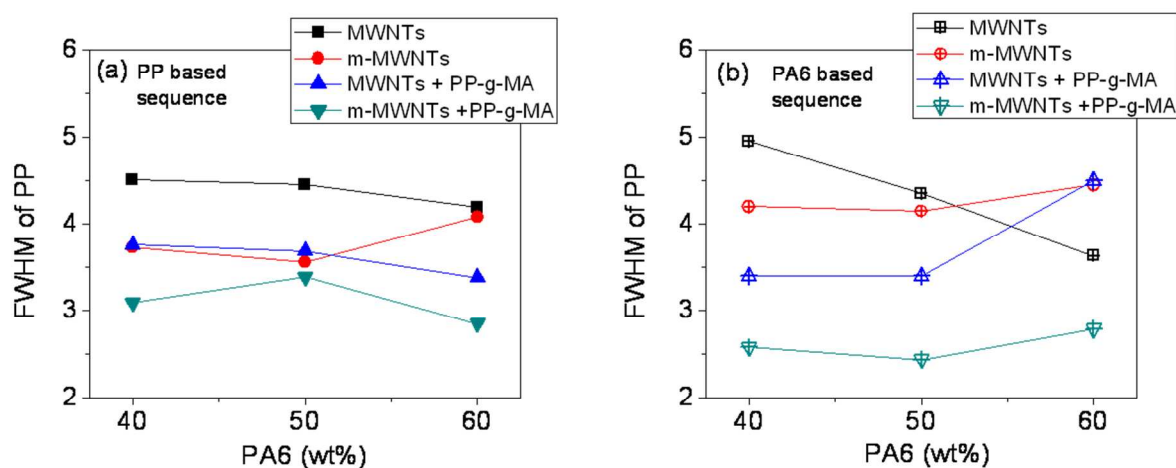

Figure 7: FWHM of PP with increasing concentration of the PA6 phase in the blends prepared via (a) 'protocol 1' and (b) protocol 2'

d. Crystallization behaviour of PP/PA6 blends in the presence of MWNTs through WAXD analysis

Fig. 8(a) shows wide angle X-ray diffraction pattern of neat PP, PP-g-MA and PA6. Neat PP shows α-crystalline phase, which exhibits the diffraction maxima at $2\theta = 14.06°$, $16.89°$, $18.52°$, $21.18°$ and $21.67°$, corresponding to (110), (040), (130), (111) and (041) reflection planes. Neat PA6 shows α-crystalline phase, which shows the diffraction maxima at $2\theta = 20.1°$ and $23.6°$, corresponding to (200), (002)/(202) reflections. The metastable γ-form is also observed at $2\theta = 21.5°$ corresponding to (001) plane. However, the peaks corresponding to PA6

phase overlap with (111) and (041) reflection planes of the PP phase, therefore, the contribution

of the peaks in this region could not be considered. Fig. 8 (b) shows X-ray diffraction pattern of

50/50 (wt/wt) PP/PA6 blend in the presence of pristine MWNTs. Incorporation of MWNTs does

not affect the crystalline structure associated with the PP phase. A similar behaviour was

reported by Park et al. for MWNTs reinforced PP composites [42]. Further, 50/50 (wt/wt)

PP/PA6 blend shows a decrease in the intensity corresponding to (110) plane and an increase in

the intensity corresponding to (040) plane as compared to pure PP indicating an enhanced

orientation along the (040) plane. In the presence of pristine MWNTs, 50/50 (wt/wt) PP/PA6

blend prepared via 'protocol 1' shows more oriented PP chains along (110) plane as compared to

the corresponding neat blend, however, lower than pure PP or PP/MWNTs composites. This

suggests that incorporation of PA6 facilitates the orientation along (040) reflection plane,

however, the presence of MWNTs facilitates orientation of PP chains along the (110) plane.

Moreover, the corresponding blend prepared via 'protocol 2' shows a decrease in the intensity

corresponding to (110) plane as compared to blend prepared via 'protocol 1'. In this case,

pristine MWNTs were initially added to the PA6 phase thus, the fraction of the migrated

MWNTs in the PP phase would be lesser than that of the blend prepared via 'protocol 1'.

Therefore, the effect of addition of PA6 phase dominates over the effect of the addition of

MWNTs in case of blend prepared via 'protocol 2'. Interestingly, addition of PA6 phase leads to

β-crystal structure formation in the PP phase, which is indicated by the presence of 2θ peak at

~16.0° and ~20.2° corresponding to (300) and (301) reflection plane respectively. Incorporation

of pristine MWNTs in the blend could enhance the β-crystal structure formation and the effect is

more prominent in case of blend prepared via 'protocol 1'. However, β-phase formation is

observed only in the 'skin' side of the injection molded samples. In the 'core' side of the sample,

it is not significant. Intensity corresponding to the α-phase is also lower in the 'core' side as compared to the 'skin' side of the blend sample. It is envisaged that injection molding process leads to higher orientation of the polymer chains in the 'skin' side of the sample due to differential cooling of the melt in the 'skin' and the 'core' side of the sample. This may enhance the growth of α-fraction of the PP phase towards a specific reflection plane in the 'skin' side of the sample. The same explanation may be extended for the β-phase formation of the PP phase in the 'skin' side of the sample. It is also to be noted that the signature due to β-crystal structure formation was not evident in the DSC analysis as 'extrudate' sample was investigated.
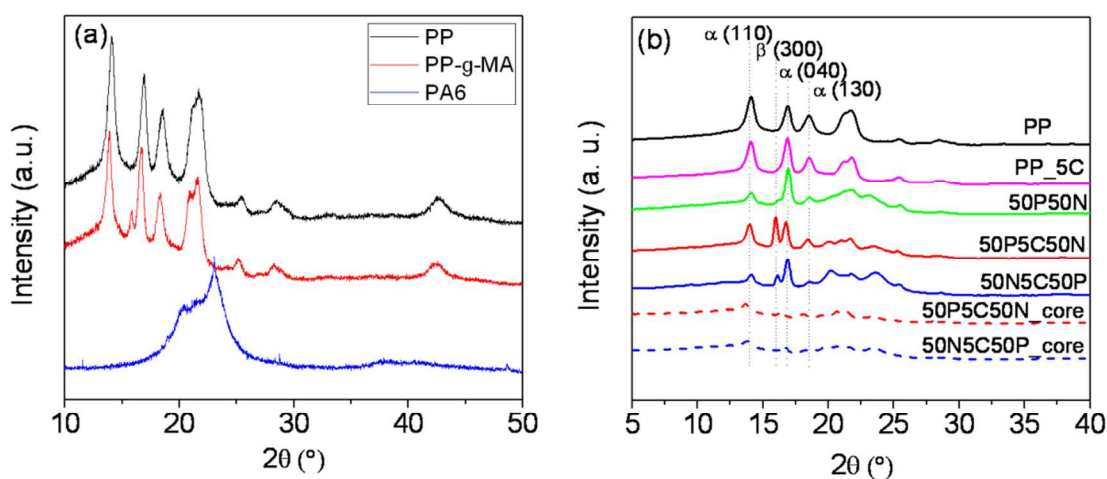

Figure 8: WAXD pattern of: (a) neat PP and neat PP-g-MA, (b) PP, PP/MWNTs, PP/PA6 blend and PP/PA6 blend with pristine MWNTs

Fig. 9 (a) depicts the X-ray diffraction pattern of PP/PA6 blend with MWNTs of varying blend composition prepared via 'protocol 1' and 'protocol 2'. In case of blend prepared via 'protocol 1', peak intensity corresponding to (110) and (040) plane increases with increasing content of the PP phase. However, in case of blend prepared via 'protocol 2', intensity corresponding to (110) plane remains almost constant, whereas, intensity corresponding to (040) plane increases with increasing content of the PP phase. Further, blend prepared via 'protocol 1'

shows higher intensity for β peak corresponding to (300) plane as compared to the corresponding

blend prepared via 'protocol 2', which suggests an alteration of viscosity ratio in the blend

prepared via 'protocol 1' and higher fraction of PA6 phase may as well involve in the 'skin' side

along with MWNTs. Fig. 9 (b) shows the X-ray diffraction pattern of PP/PA6 blend with m-

MWNTs as a function of varying blend composition prepared via 'protocol 1' and 'protocol 2'. It

shows that incorporation of m-MWNTs affects the crystalline structure of the PP phase in a

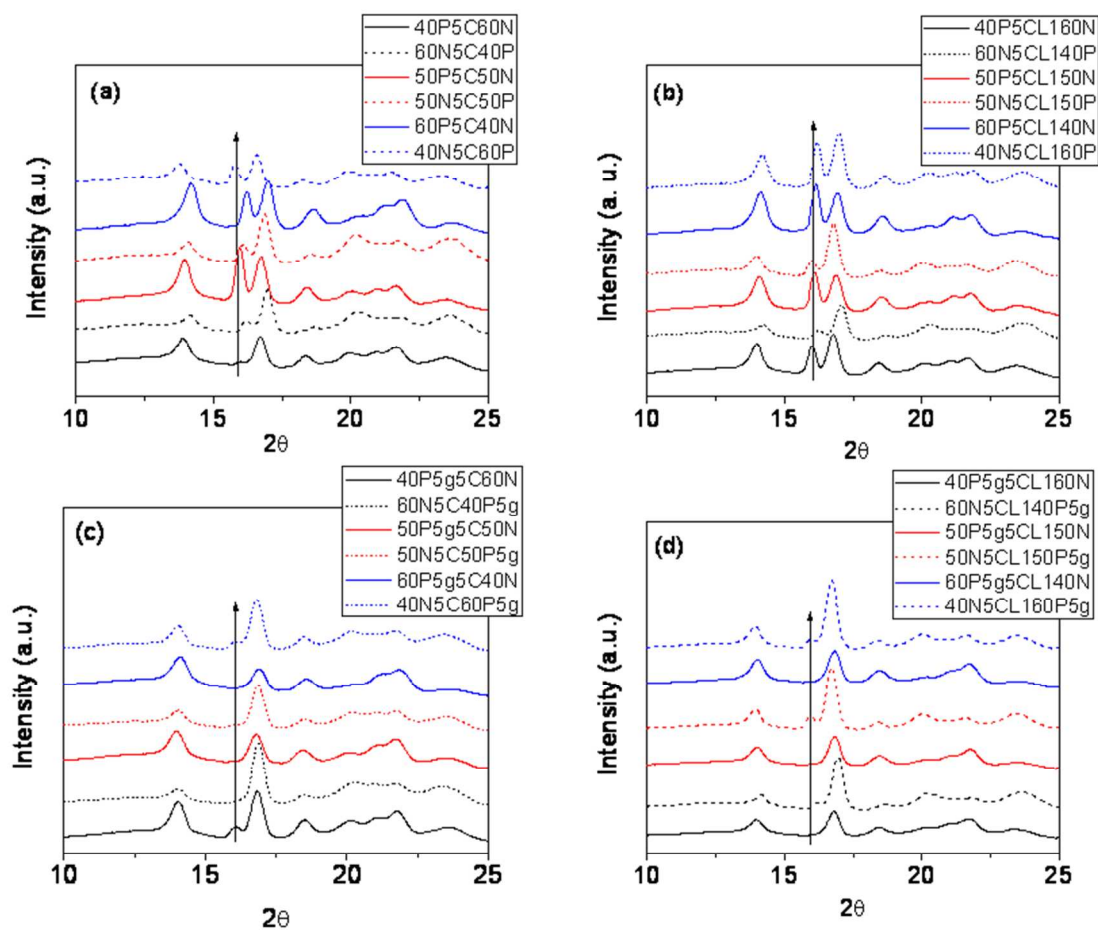blend in a similar fashion in the blend with pristine MWNTs.

Figure 9: WAXD pattern of PP in 50/50 (wt/wt) PP/PA6 blend with (a) pristine MWNTs, (b) m- MWNTs, (c) pristine MWNTs and PP-g-MA,(d) m-MWNTs and PP-g-MA

Fig. 9 (c) and (d) exhibit the X-ray diffraction pattern of sequentially mixed PP/PA6

blend with pristine and m-MWNTs of different blend composition in the presence of PP-g-MA.

β-phase formation is not significant when PP-g-MA is incorporated into the system. In case of blend prepared via 'protocol 1', β-crystal structure formation is not observed in the presence of PP-g-MA irrespective of the blend with pristine/m-MWNTs. Further, a small signature of the β-phase is observed in case of blend prepared via 'protocol 2'. Moreover, in case of blend prepared via 'protocol 2', peak intensity corresponding to (040) plane is higher as compared to blend prepared via 'protocol 1'.
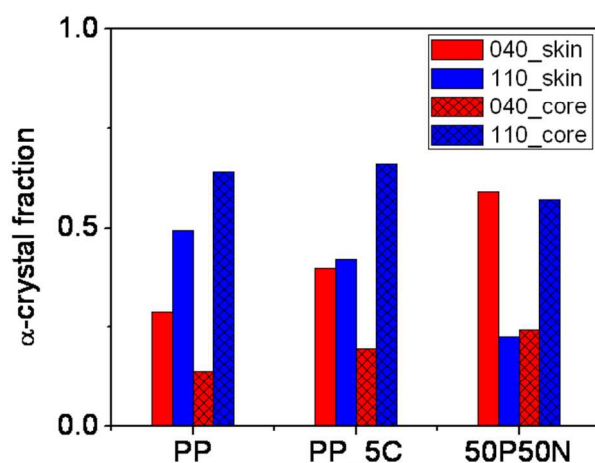

Figure 10: α -fraction corresponding to (040) and (110) plane of PP, PP with 5 wt% MWNTs and 50/50 (wt/wt) PP/PA6 blend

The relative content of α and β-crystal in the PP phase in the blend is calculated according to Turner–Jones formula [43], which has been described in the literature as follows:

$$K_\beta = \frac{H_{300}}{H_{110} + H_{040} + H_{130} + H_{300}} \dots \dots \dots \dots \dots (1)$$

where, H_{110}, H_{040} and H_{130} are the intensity of the peaks corresponding to (110), (040) and (130) reflections of α-crystal of the PP phase, appearing at $2\theta \sim 14.1°$, $16.9°$, and $18.5°$ respectively,

and H_{300} is the intensity of the (300) reflection of the β -crystal of the PP phase at 2θ ~ 16.0°. It is

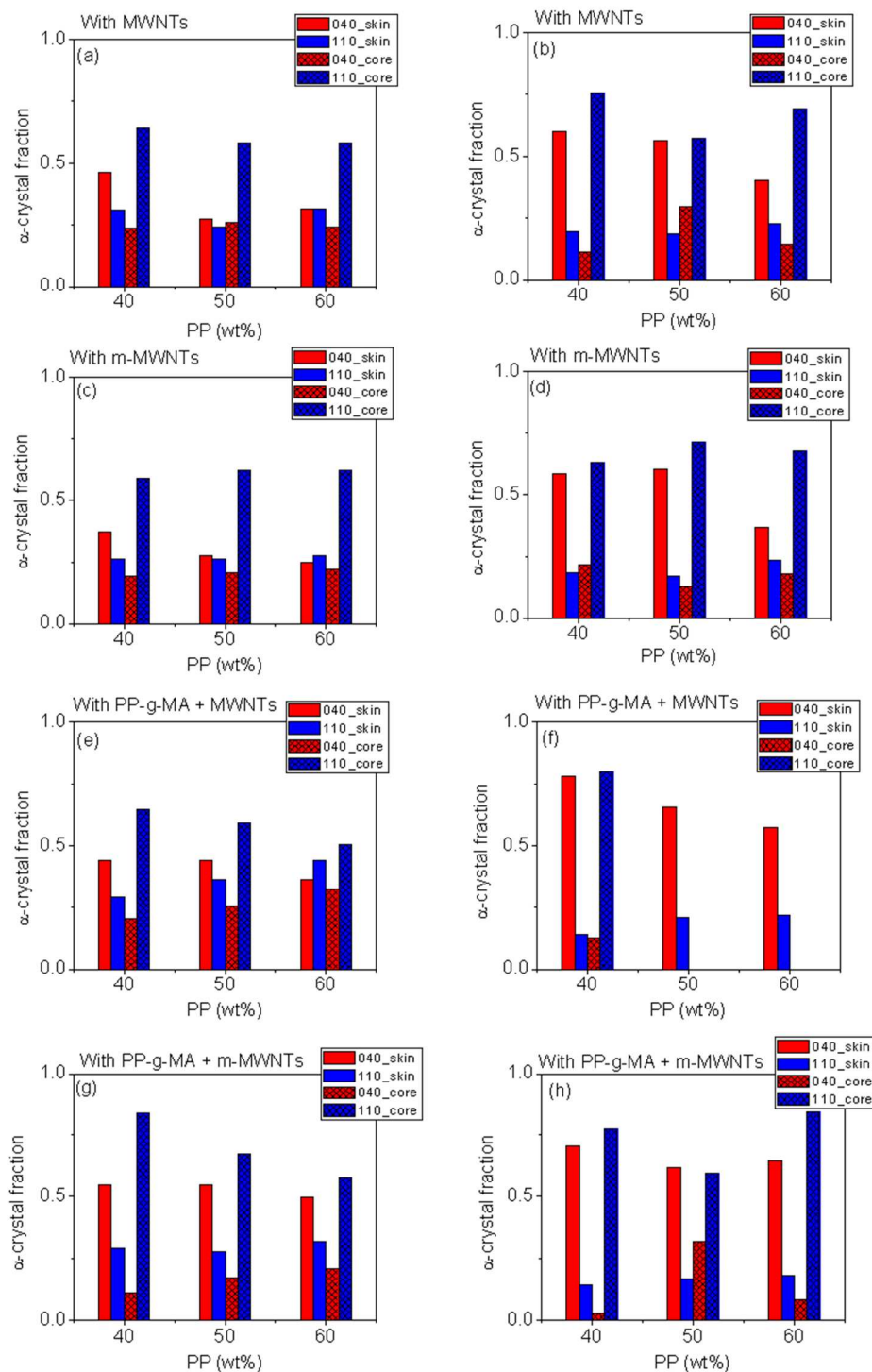assumed that if β -crystal is absent in i-PP, $K_β= 0$; if i-PP consists of 100% β-crystal, then $K_β= 1$.

Figure 11: α-fraction of the PP phase in PP/PA6 blends with pristine MWNTs prepared via (a) 'protocol 1' and (b) 'protocol 2';with m-MWNTs prepared via (c) 'protocol 1' and (d) 'protocol 2';with PP-g-MA and pristine MWNTs prepared via (e) 'protocol 1' and (f) 'protocol 2'; with PP-g-MA and m- MWNTs prepared via (g) 'protocol 1' and (h) 'protocol 2'

Fig. 10 depicts the α-fraction corresponding to (040) and (110) planes of neat PP, PP with 5 wt% pristine MWNTs and 50/50 (wt/wt) PP/PA6 blend for the 'skin' and 'core' side of the injection molded samples. It is observed that α-fraction corresponding to (040) plane is lesser than α-fraction corresponding to (110) plane in both 'skin' side and 'core' side of neat PP. In the presence of MWNTs or PA6, α-fraction corresponding to (040) plane increases and (110) plane decreases in the 'skin' side. This suggests that in the presence of MWNTs or PA6, PP chains orient themselves along the (040) plane in the 'skin' side of the injection molded sample.
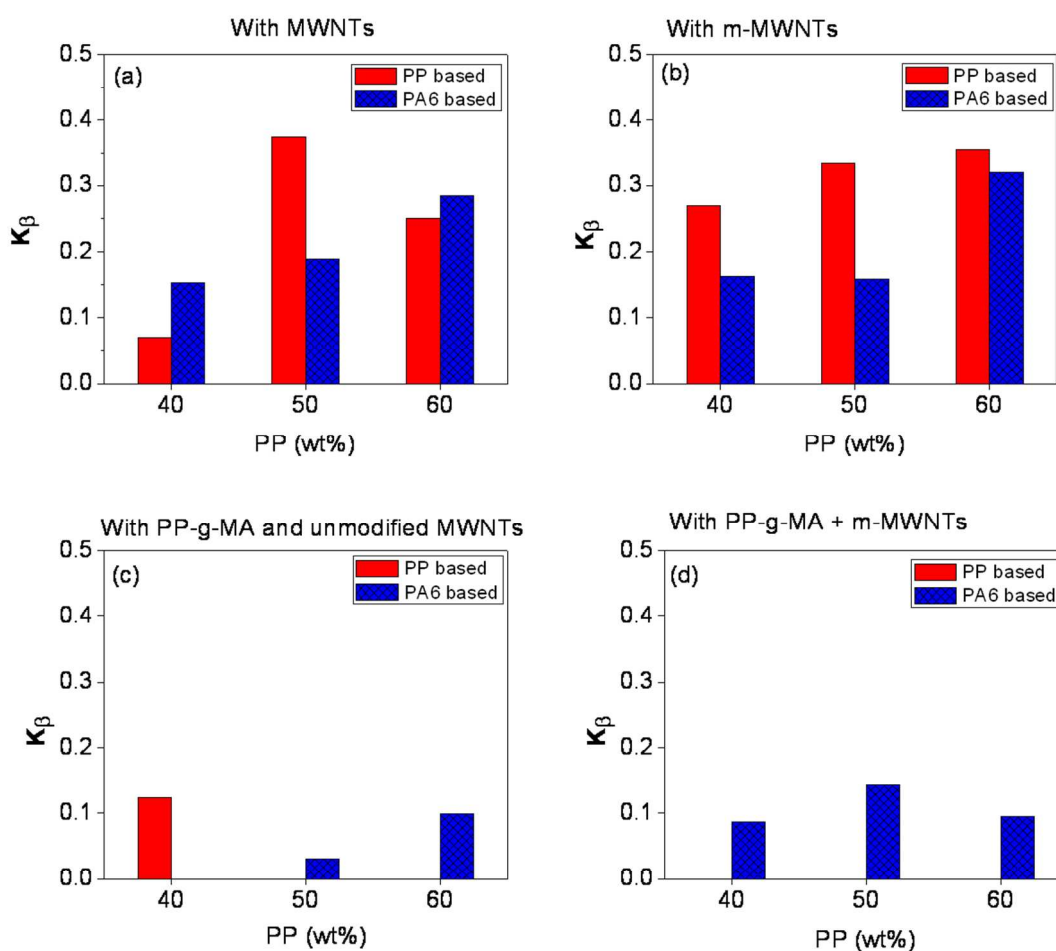
Figure 12: β-fraction of the PP phase in PP/PA6 blends with (a) pristine MWNTs (b) m-MWNTs (c) PP-g-MA and pristine MWNTs and (d) PP-g-MA and m-MWNTs prepared via 'protocol 1' and 'protocol 2'

Fig. 11 (a) and (b) show the α-fraction corresponding to (040) and (110) planes in PP/PA6 blend with pristine MWNTs as a function of blend composition. It is observed that for the 'skin' side, α-fraction corresponding to (040) plane is higher than (110) plane and for the 'core' side, α-fraction corresponding to (040) plane is lesser than (110) plane. With increasing concentration of the PP phase, α-fraction corresponding to (040) plane decreases and (110) plane increases for the 'skin' side of the sample. However, an opposite trend is observed for the 'core' side of the sample. A similar behaviour is observed in case of blend with m-MWNTs and also in the blend with pristine/m-MWNTs in the presence of PP-g-MA [Fig 11 (c), (d), (e), (f), (g), and (h)]. However, the difference between the two sequences is quite significant. In all the cases, 'protocol 2' leads to the majority of the PP chains to be oriented along a preferred direction [(040) plane in case of the 'skin' side and (110) plane in case of the 'core' side], whereas, blends prepared via 'protocol 1' lead to a similar extent of orientation of the PP chains in two different planes as observed from the α-crystal fraction calculation of the PP phase in both the planes. Based on the above observations, it may be commented that the orientation of the PP chain is predominantly influenced by the viscosity ratio of the blend; the lower viscous phase may tend to form the 'skin' in the injection molded sample.

Fig. 12 (a) and (b) show the β-crystal fraction (K_β) in case of blend with pristine MWNTs and m-MWNTs. K_β increases with increasing content of the PP phase in the blend with pristine MWNTs. However, in the presence of m-MWNTS, blends prepared via 'protocol 1' show higher β-crystal fraction as compared to the corresponding blends prepared via 'protocol 2'. β-peak corresponding to the PP phase disappears in the majority of the blends prepared via 'protocol 1' (appears only in case of 40P5g5C60N) on incorporation of PP-g-MA [Fig. 12 (c)]. Further, β-

peak is observed in the blends prepared via 'protocol 2' (except 40P5g5C60N composition), however, K_β is much lesser as compared to the corresponding uncompatibilized blend. A similar trend is observed in case of blend with PP-g-MA and m-MWNTs [Fig. 12 (d)]. In the presence of PP-g-MA along with m-MWNTs, only the blends prepared via 'protocol 2' show β-crystal structure formation, however, the value is much lesser (0.1) than the corresponding uncompatibilized blend. Therefore, presence of PP-g-MA could suppress the β-crystal structure formation to some extent.

Crystal size for the (110) and (040) planes are calculated from the XRD data using Scherrer formula $t = \frac{0.9\lambda}{\beta \cos\theta}$, where t is the crystallite size in nm, β is broadening of diffraction line at full width at half maxima (FWHM), θ was obtained from corrected peak position, 2θ and λ is the wavelength of CuKα radiation i.e. 0.154 nm [44]. Instrumental broadening of the XRD peaks was corrected using the following equation: $\beta = \sqrt{\beta_m{}^2 - \beta_s{}^2}$, where β_s is the system broadening, which is determined by polycrystalline silicon standard sample and β_m is the broadening of the blend sample.

Crystal size of pure PP is 13.4 nm and 17.3 nm for the (110) and (040) crystal planes respectively. When PA6 is added to the PP phase [50/50 (wt/wt) PP/PA6 blends], the crystal size has increased to 15.8 nm and 22.9 nm respectively. Fig. 13 shows the crystal size of the PP phase with increasing concentration of the PA6 phase for (110) plane of PP in the blends prepared via (a) 'protocol 1' and (b) protocol 2' and for (040) plane of PP in the blends prepared via (c) 'protocol 1' and (d) protocol 2'. The crystal size in the PP/PA6 blends with pristine/m-MWNTs in the presence or absence of PP-g-MA varies from 13-24 nm, which is almost invariant with the concentration of the PA6 phase. However, crystal size of the PP phase is at the lower end [13-18 nm for (110) plane and 17-24 nm for (040) plane] in case of the blends prepared via 'protocol 1'.

Blends prepared via 'protocol 2' exhibit the variation of the crystal size of PP, which lie between

16-20 nm for (110) plane and (20-24) nm for (040) plane. Crystal size of the PA6 phase could

not be calculated because the characteristic peaks of the PA6 phase merge with the (130) peak of

the PP phase.
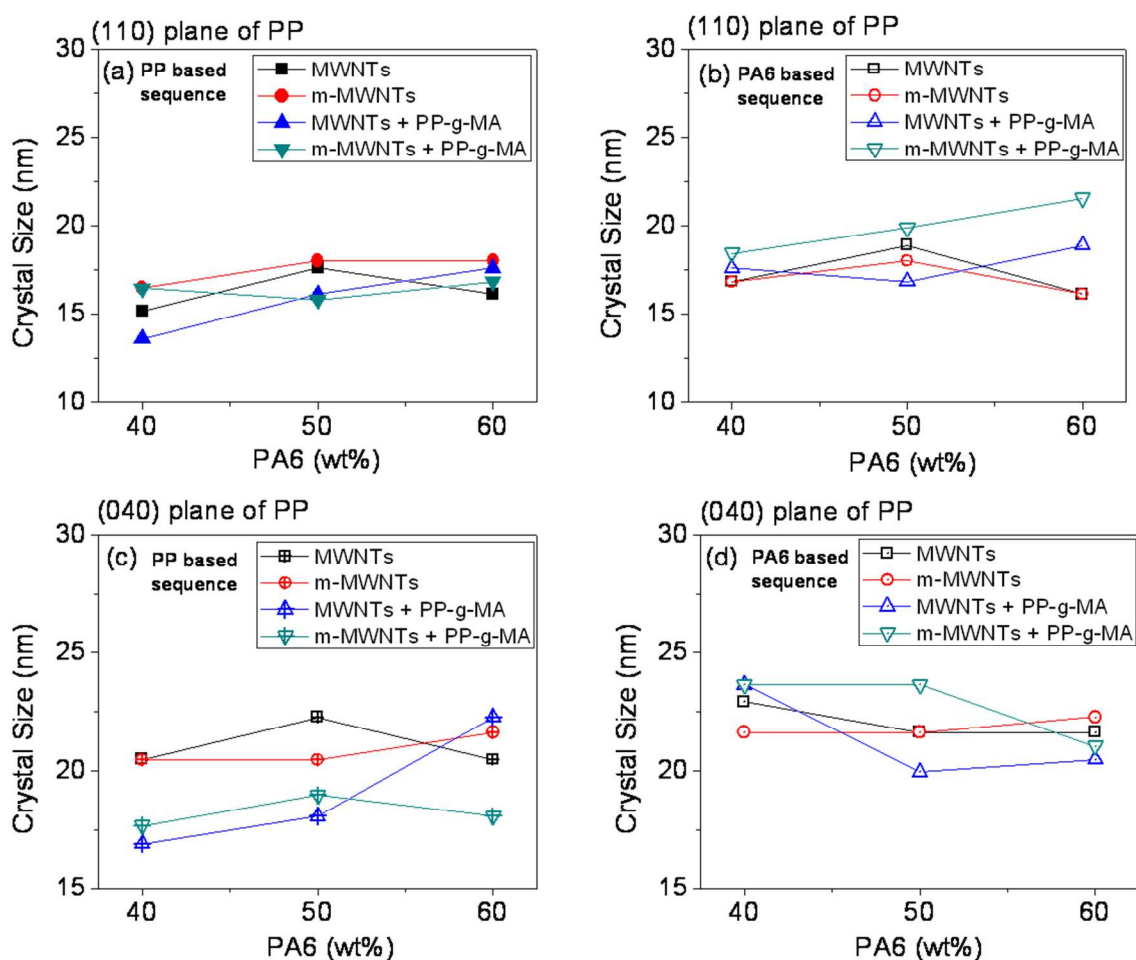
Figure 13: Crystal size of the PP phase with increasing concentration of the PA6 phase for (110) plane of PP in the blends prepared via (a) 'protocol 1' and (b) protocol 2' and for (040) plane of PP in the blends prepared via (c) 'protocol 1' and (d) protocol 2'

The strain could be estimated using the Williamson-Hall plots [44-45], however, in our

case it has been analyzed with the two peaks corresponding to the PP phase. Rest of the peaks is

overlapped with the peaks of both the PP and the PA6 phase. Therefore, the slope of the plot

31

could not provide us the accurate strain values and hence, the strain measurements are not shown in this paper.

e. X-ray bulk texture analysis of PP/PA6 blends in the presence of MWNTs

Fig. 14 exhibits the pole figures of X-ray bulk texture carried out for (110), (040), (130) and (041) crystalline planes of 50/50 PP/PA6 blends with pristine MWNTs. Pole figures for neat PP and neat 50/50 PP/PA6 blend are also plotted as references. In these figures, the extent of orientation of PP chains towards a specific crystalline plane is indicated through contour plot of varying colour, each contour level designates the extent of crystal texture. This point is brought out by the respective $f(g)_{max}$ values, which are listed in Table 2. All the figures are plotted in same scale. It is to be noted that intensity vs. 2θ diffraction pattern in WAXD analysis earlier indicates that the intensity corresponding to (110) crystalline plane is higher than the intensity corresponding to (040) crystalline plane while intensity of (040) crystalline plane is higher than the intensity corresponding to (130) crystal plane in case of neat PP [Fig. 8 (b)]. However, in case of neat blend as well as blend with MWNTs, the intensity corresponding to (040) crystalline plane becomes higher than both the intensity corresponding to (110) and (130) crystalline planes [Fig. 8 (b)]. A similar trend is observed from the respective pole figures as well [Fig. 13]. Neat blend of 50/50 PP/PA6 shows highest extent of crystal structure along (040) plane as compared to neat PP and 50/50 PP/PA6 blend with pristine MWNTs. However, in case of blend with pristine MWNTs, extent of orientation along (040) plane is lesser than that of the neat blend.

Figure 13: Pole figure of (040), (041), (110) and (130) crystalline planes for the PP phase of (a) neat PP (b) neat 50/50 (wt/wt) PP/PA6 blend, 50/50 (wt/wt) PP/PA6 blend with pristine MWNTs prepared via(c) 'protocol 1' and (d) 'protocol 2'

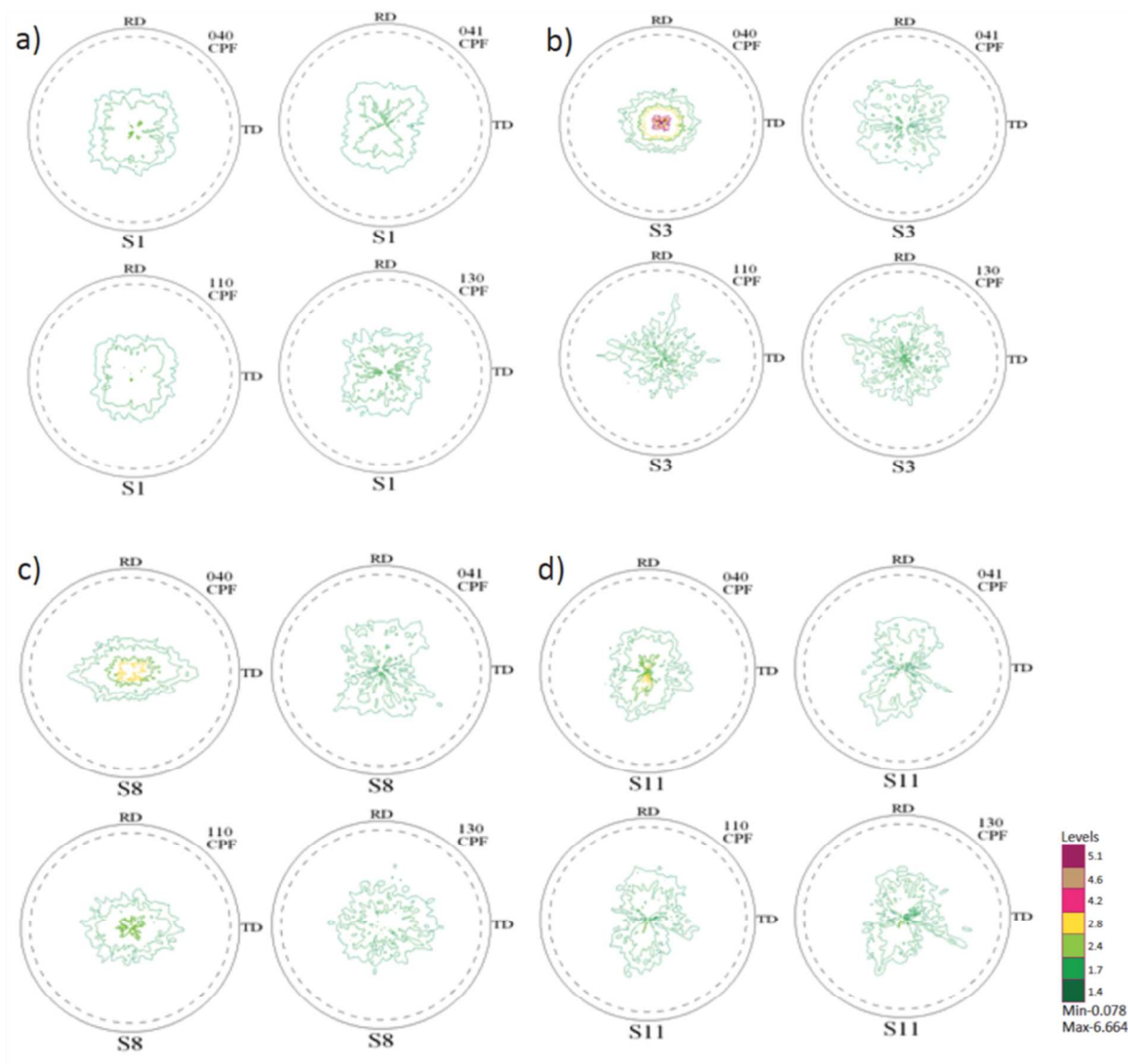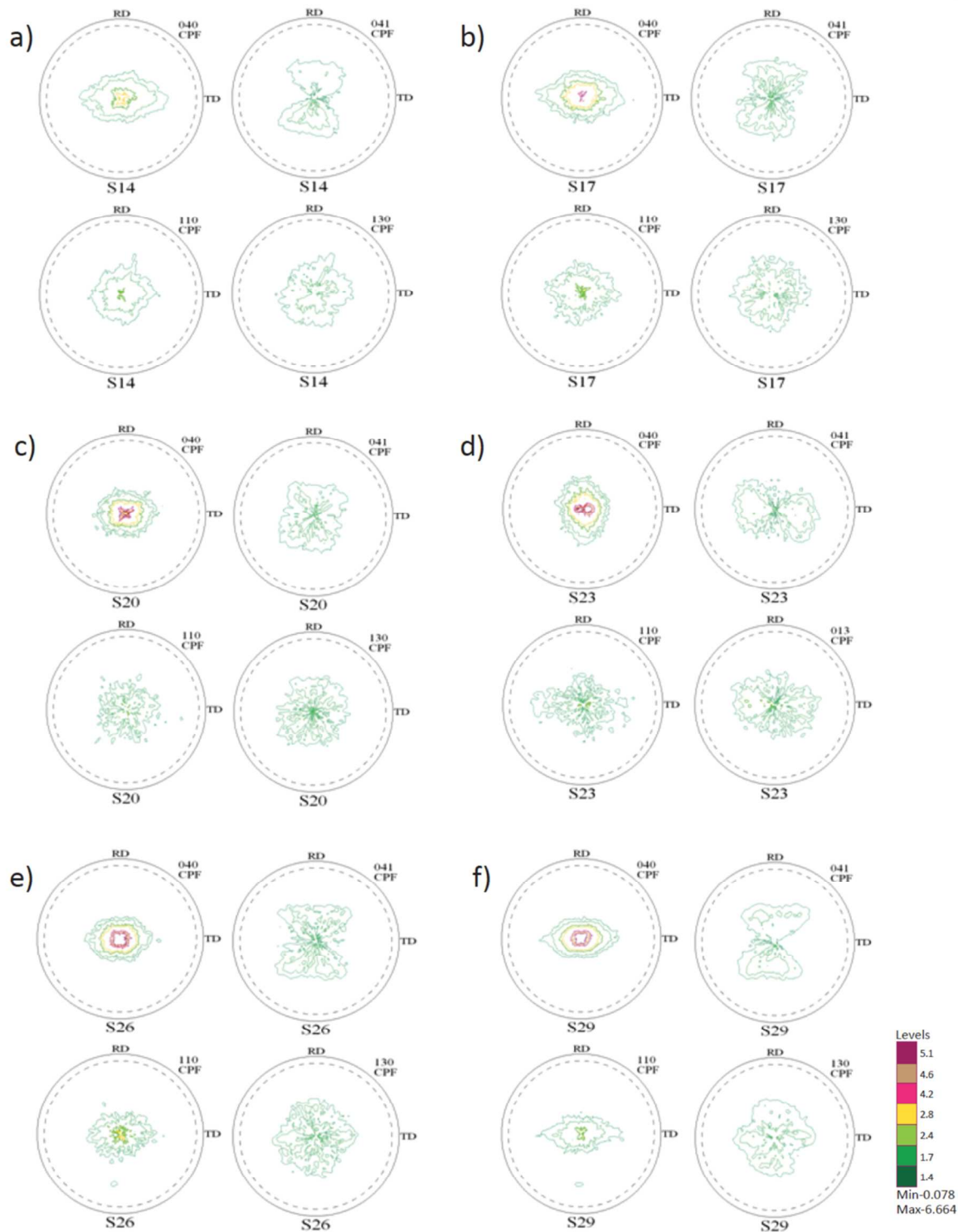**Figure 14: Pole figure of (040), (041), (110) and (130) crystalline planes for the PP phase of 50/50 (wt/wt) PP/PA6 blend with m- MWNTs prepared via (a) 'protocol 1' and (b) 'protocol 2'; with PP-g-MA and pristine MWNTs prepared via (c) 'protocol 1' and (d) 'protocol 2'; with PP-g-MA and m- MWNTs prepared via (e) 'protocol 1' and (f) 'protocol 2'**

Fig. 14 exhibits the pole figures of X-ray bulk texture carried out for (110), (040), (130) and (041) crystalline planes of the PP phase in 50/50 PP/PA6 blend with m-MWNTs in the presence and absence of PP-g-MA. All the samples exhibit weak crystallographic texture of the PP chains in all the four crystalline planes. All the samples exhibit higher extent of crystalline structure along (040) plane as compared to other crystallographic planes. In case of blend with m-MWNTs [Fig. 10 (a) and (b)], orientation along (040) plane is observed to be more in case of blend prepared via 'protocol 2'. In case of blend with PP-g-MA (both with pristine and m-MWNTs), the extent of orientation of the PP chains increases along (040) and (110) plane as compared to the corresponding uncompatibilized blends. Therefore, it is clear that the presence of PP-g-MA favours the α-crystal structure formation, henceforth, suppresses β-crystal formation in compatibilized blends. All the above observations are in accordance with the α-fraction plots, which has been discussed earlier [Fig. 11 (c)-(h)].

The texture indices are calculated from the orientation distribution function. Texture indices as represented as $\int f(g)^2 dg$ has been considered as an indicator of relative anisotropy or texturing where, $.f(g)$ is the orientation intensity and $dg = \frac{\sin\phi \, d\phi_1 \, d\phi \, d\phi_2}{4\pi^2}$ in case of monoclinic PP [46-48]. The corresponding values of texture indices are summarized in Table 3. PP/PA6 blends with pristine MWNTs and PP-g-MA prepared via 'protocol 2' shows the most anisotropic structure. This may be due to the alteration of viscosity ratio of the blend phases, wherein the lower viscous phase may tend to form the 'skin' in the injection molded sample. PA6 phase is less viscous as compared to the PP phase. In case of blends prepared via 'protocol 2', MWNTs are mainly in the PA6 phase and hence, enhancing the melt-viscosity of the PA6 phase. However, in the presence of PP-g-MA, (wherein, PP-g-MA is incorporated in the PP

phase) the melt-viscosity of the PP phase is increased. PP chain is predominantly influenced by the viscosity ratio of the blend, all other samples exhibited similar values of texture indices.

Residual stresses of the blend samples were measured through standard d-Sin$^2\psi$ method [44,49-51]. The values are provided in Table 4. The normal stress (σ_{11}) and shear stress (τ_{13}) components of the residual stress tensor do not show any particular trend or effect of MWNTs/m-MWNTs. Fig. 15 shows a schematic representation of crystallization of PP chains in PP/PA6 blends with (a) pristine MWNTs (b) m- MWNTs (c) PP-g-MA and pristine MWNTs and (d) PP-g-MA and m-MWNTs prepared via 'protocol 1' and 'protocol 2'. It exhibits the migration of MWNTs to one phase to another phase and also shows how the 'agglomerated'/'individualized' MWNTs act as a heteronucleating agent and affect the crystallization behaviour of the polymer chains and the growth of crystals.
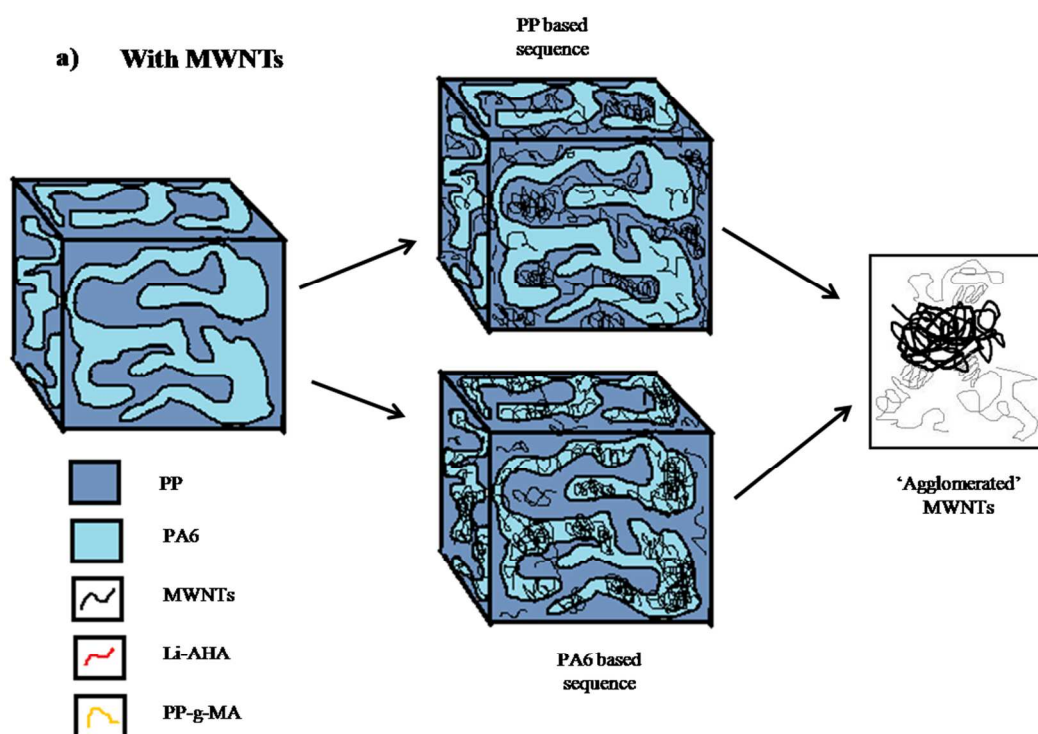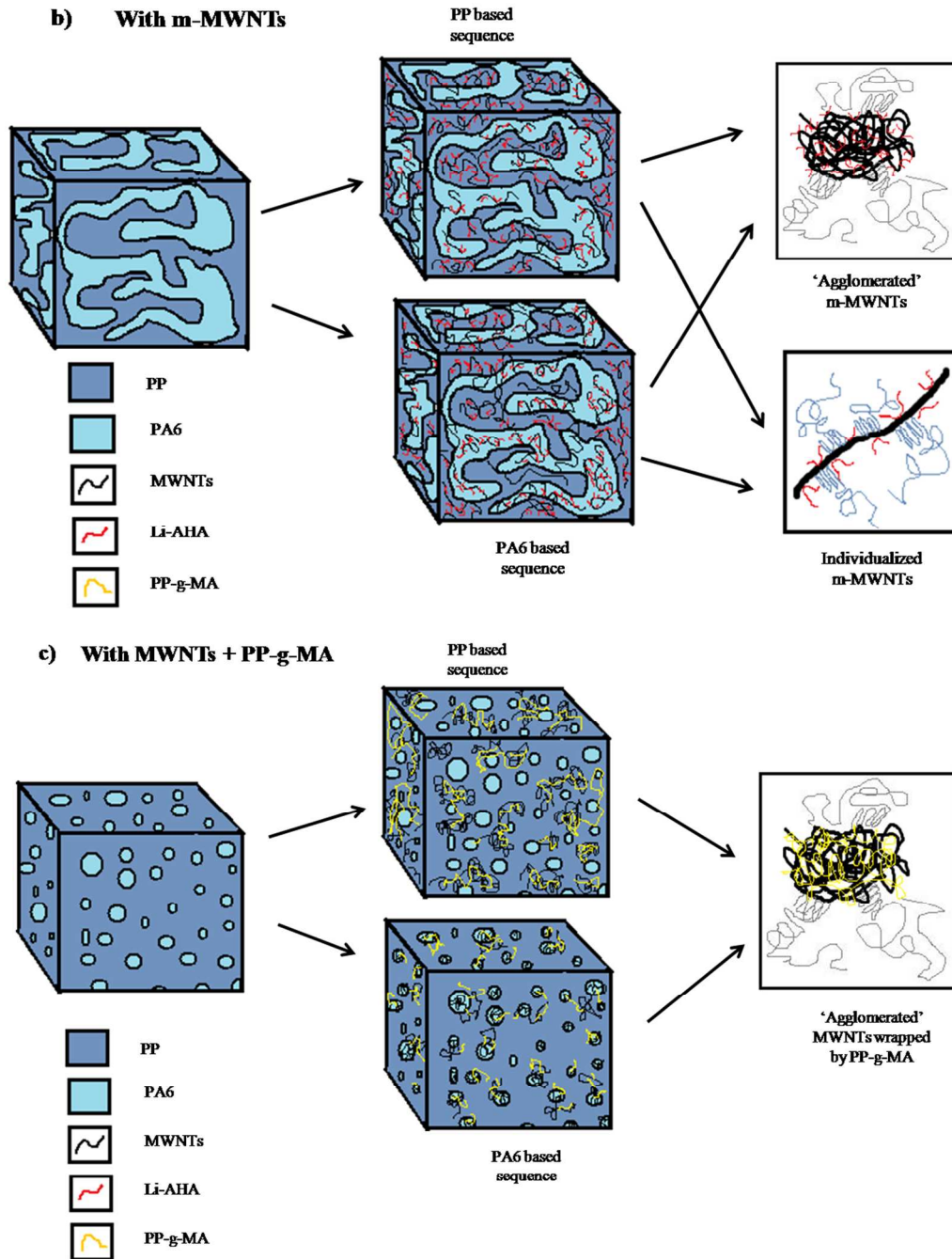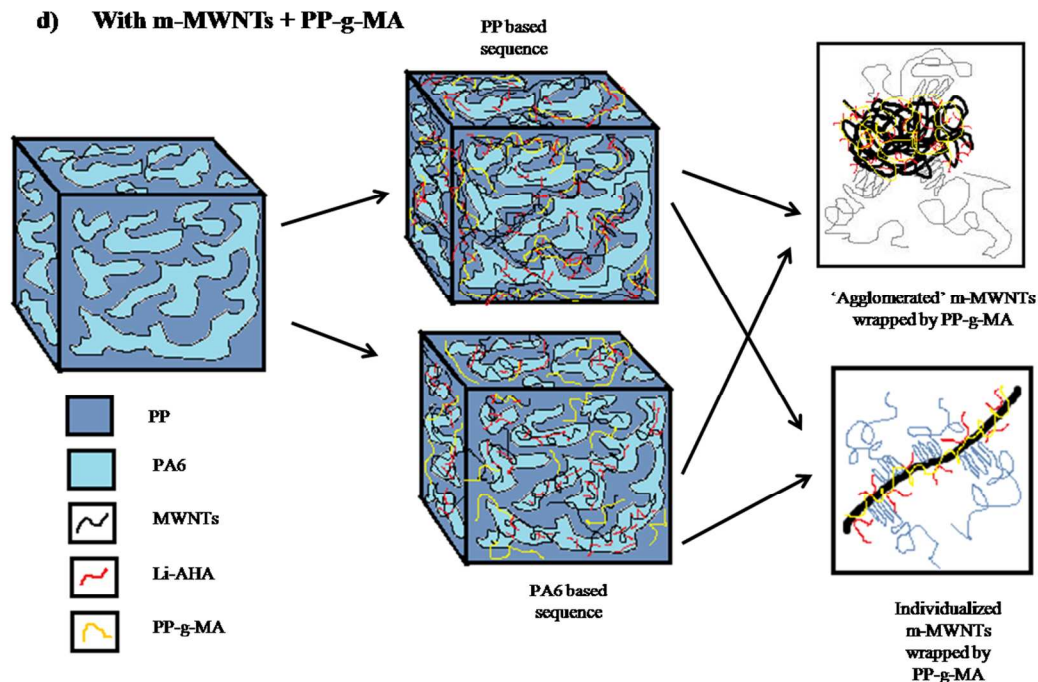
Figure 15: Schematic representations of crystallization of PP chains in PP/PA6 blends with (a) pristine MWNTs (b) m- MWNTs (c) PP-g-MA and pristine MWNTs and (d) PP-g-MA and m-MWNTs prepared via 'protocol 1' and 'protocol 2'

Conclusions

Crystallization studies have been carried out for 40/60-60/40 (wt/wt) PP/PA6 blends with pristine and m-MWNTs in the presence of the compatibilizer (PP-g-MA). In the presence of PA6, T_c of the PP phase has increased significantly indicating the hetero-nucleating action of the PA6 phase. Incorporation of pristine MWNTs in the blend has led to further increase in T_c of the PP phase. Further, the PA6 phase in the blend in the presence of MWNTs has exhibited double exothermic crystallization peak due to 'trans-lamellar crystalline' structure formation by the PA6 phase on the 'individualized' MWNTs surface and also due to the hetero-nucleating action by 'agglomerated' MWNTs. The formation of 'trans-crystalline lamellar' structure of the PA6 phase was facilitated in case of blends where MWNTs were initially added to the PA6 phase. The corresponding blend with m-MWNTs has shown a decrease in T_c of the PP phase as compared to

blend with pristine MWNTs both in the presence and the absence of PP-g-MA. Incorporation of PP-g-MA has led to higher T_c of the PP phase as compared to uncompatibilized blend. A second crystallization peak near to the PP phase in some of the blend compositions has been observed due to the fractionated crystallization of the PA6 droplets in the presence of PP-g-MA.

WAXD analysis has shown that addition of PA6 phase has facilitated the orientation of the PP chains along the (040) reflection plane, whereas the presence of MWNTs has oriented the PP chains along the (110) reflection plane. Further, incorporation of the PA6 phase has led to β-crystalline structure formation of the PP phase which has been indicated by the diffraction peak at 2θ~ 16° and ~20.2° corresponding to the (300) and (301) reflection plane. Incorporation of pristine/m-MWNTs in the PP/PA6 blend has retained the β-crystal structure formation. However, β-phase formation was observed only in the 'skin' side of the injection molded samples. In the 'core' side it was absent. Further, intensity of α-peaks was lower in the 'core' side than the 'skin' side of the sample. The addition of PP-g-MA has suppressed the β-crystalline structure formation. Further, X-ray bulk texture analysis has confirmed that incorporation of PA6 and MWNTs has affected the orientation of the PP chains along preferred directions and the experimental observations were in accordance with the WAXD analysis.

In brief, the crystallization behaviour of the PP as well the PA6 phase has been significantly influenced by the presence of MWNTs in the blend. This has manifested in variation of T_c, α-crystalline fraction, β-fraction and the orientation of the PP phase towards a specific crystalline plane in the blend prepared via a specific mixing sequence. Moreover, it has also manifested in a variation of H_1/H_2 ratio of the double exothermic crystallization peak of the PA6 phase in the blend prepared via a specific mixing sequence.

Table 1: Sample Codes along with the compositions of PP/PA6 blend with pristine and m-MWNTs in the presence and the absence of PP-g-MA

CODE	PP (P) wt%	MWNT (C) wt%	Li-AHA (L) wt%	PP-g-MA (g) wt%	PA6 (N) wt%
Samples prepared by sequential mixing technique					
xN5CyP PA6 based sequence	x(40-60)	5			y(60-40)
xP5CyN PP based sequence	x(40-60)	5			y(60-40)
xN5CL1yP PA6 based sequence	x(40-60)	5	5		y(60-40)
xP5CL1yN PP based sequence	x(40-60)	5	5		y(60-40)
xN5CyP5g PA6 based sequence	x(40-60)	5		5	y(60-40)
xP5g5CyN PP based sequence	x(40-60)	5		5	y(60-40)
xN5CL1yP5g PA6 based sequence	x(40-60)	5	5	5	y(60-40)
xP5g5CL1yN PP based sequence	x(40-60)	5	5	5	y(60-40)

Table 2: f(g)$_{max}$ and f(g)$_{min}$ values of the various compositions of PP/PA6 blend with pristine and m-MWNTs in the presence and the absence of PP-g-MA obtained from pole figure

Sample Code	f(g)$_{max}$	f(g)$_{min}$
PP	2.592	0.115
50P50N	2.438	0.069
50P5C50N	2.156	0.119
50N5C50P	2.201	0.105
50P5CL150N	2.017	0.169
50N5CL150P	2.171	0.122
50P5g5C50N	2.748	0.14
50N5C50P5g	4.807	0.123
50P5g5CL150N	1.914	0.108
50N5CL150P5g	2.341	0.137

Table 3: Texture Index values of the various compositions of PP/PA6 blend with pristine and m-MWNTs in the presence and the absence of PP-g-MA

Sample Code	Texture Index
PP	3.5
50P50N	3.4
50P5C50N	2.4
50N5C50P	2.7
50P5CL150N	2.8
50N5CL150P	3.3
50P5g5C50N	3.0
50N5C50P5g	9.0
50P5g5CL150N	2.5
50N5CL150P5g	3.0

Table 4: Residual stress values of the various compositions of PP/PA6 blend with pristine and m-MWNTs in the presence and the absence of PP-g-MA

	110 plane		040 plane		130 plane		041 plane	
	σ_{11}(MPa)	τ_{13}(MPa)	σ_{11}(MPa)	τ_{13}(MPa)	σ_{11}(MPa)	τ_{13}(MPa)	σ_{11}(MPa)	τ_{13}(MPa)
PP	4.5	0.6	-3.1	0.0	5.4	1.2	13	1.1
50P50N	11.5	1.4	24.1	2.8	5.7	0.8	12.6	1.5
50P5C50N	7.0	1.5	9.8	1.6	7.7	2.0	24.2	9.4
50N5C50P	7.4	1.3	6.1	1.0	7.7	1.7	22.2	3.7
50P5CL150N	20.4	3.4	-4.2	0.8	35.3	4.4	21.8	3.2
50N5CL150P	12.2	1.2	11.7	2.1	29.3	3.8	14.9	1.5
50P5g5C50N	20.2	4.2	9.6	1.6	56.1	16.9	58.8	11.5
50N5C50P5g	49.1	13.0	73	12.7	59.4	12.8	26.5	4.3
50P5g5CL150N	16.6	2.7	18.3	3.9	-6.0	2.9	65.2	8.5
50N5CL150P5g	8.0	1.4	35.8	7.1	53.3	6.7	64.4	9.3

References

1. F. Ide and A. Hasegawa, *J Appl. Polym. Sci.* 1989, **18**, 963-974.

2. S. J. Park, B. K. Kim, H. M. Jeong, *Eur Polym J* 1990, **26**, 131-136.

3. H. S. Moon, B.K. Ryoo, J. K. Park, *J Polym. Sci. Part B: Polym. Phys.* 1994, **32**, 1427-1435.

4. S. N. Sathe, S. Devi, G. S. S Rao, K. V. Rao, *J Appl. Polym. Sci.* 1996, **61**, 97-107.

5. I. Campoy, J. M. Arribas, M. A. M. Zaporta, C. Marco, M. A. Gómez, J. G. Fatou, *Eur. Polym. J* 1995, **31**, 475-480.

6. C. Marco, G. Ellis, M. A. Gómez, J. G. Fatou, J. M. Arribas, I. Compoy, *J Appl. Polym. Sci.* 1997, **65**, 2665-2677.

7.   S. H. Jafari, A. K. Gupta, *J Appl. Polym. Sci.* 1999, **71**, 1153-1161.

8.   C. Marco, E. P. Collar, S. Areso, J. M. Garcia-Martinez, *J Polym. Sci. Part B: Polym. Phys.* 2002, **40**,1307-1315.

9.   M. Feng, F.L. Gong, C. G. Zhao, G.M. Chen, S. M. Zhang, M. S. Yang, *J Polym. Sci. Part B: Polym. Phys.* 2004, **42**, 3428-3438.

10.   A. Menyhárd, J. Varga, A. Liber, G. E. Belina, *Polym. J* 2005, **41**, 669-677.

11.   D. Campbell, M. M. Qayyum, *J Polym. Sci. Part B: Polym. Phys.* 1980, **18**, 83-93.

12.   J. Varga, J. J. Karger-Kocsis, *J Polym. Sci. Part B: Polym. Phys.* 1996, **34**, 657-670.

13.   B. Na, M. Guo, J. Yang, H. Tan, Q. Zhang, Q. Fu, *Polym. Int.* 2006, **55**, 441-448.

14.   P.L. Beltrame, A. Castelli, M. Canauz, *Macromol. Chem. Phys.* 1995, **196**, 2751-2766.

15.   A. González-Montiel, H. Keskkula, D.R. Paul, *J Polym. Sci. Part B: Polym. Phys.* 1995, 33, 1751-1767.

16.   A. González-Montiel, A. Keskkula, D.R. Paul, *Polymer* 1995, **36**, 4605-4620.

17.   A. Menyhárd, J. Varga, *Eur. Polym. J* 2006, **42**, 3257-3268.

18.   A. R. Bhattacharyya, T.V. Sreekumar, T. Liu, S. Kumar, L.M. Ericson, R.H. Hauge, R. E. Smalley, *Polymer* 2003, **44**, 2373-2377.

19.   S. Zhang, M.L. Minus, L. Zhu, C. Wong, S. Kumar, *Polymer* 2008, **49**, 1356-1364.

20.   J. Varga, *J Macromol. Sci. Part B: Polym. Phys.* 2002, **41**, 1121-1171.

21.   C. Grein, *Adv. Polym. Sci.* 2005, **188**, 43-104.

22.   A. Menyhárd, J. Varga, G. Molnár, *J.Ther. Anal. Cal.* 2006, **83**, 625-630.

23.   J. Varga, *J Thermal. Anal.* 1989, **35**, 1891-1912.

24.   J. Varga, A. Menyhárd, *J Ther. Anal. Cal.* 2003, **73**, 735-743.

25.   N. Mukhopadhyay, A. R. Bhattacharyya, A. Panwar, P. Pötschke, (manuscript under preparation).

26.   A. V. Poyekar, A. R. Bhattacharyya, A. S. Panwar, G. P. Simon, *Polym. Eng. and Sci.* (2014) (in press).

27.   A. V. Poyekar, A. R. Bhattacharyya, A. S. Panwar, G. P. Simonand D. S. Sutar, *ACS Appl. Mater. Interfaces*, 2014, **6**, 11054–11067.

28.   R. A. Khare, A. R. Bhattacharyya, A. R. Kulkarni, *J of Appl. Polym. Sci.* 2011, **120**, 2663-2672.

29.   K. Pawlik, P. Ozga, LaboTex: The Texture Analysis Software, Göttinger Arbeitenzur Geologie und Paläontologie, SB4, 1999.

30.   H. J. Bunge, Texture Analysis in Materials Science—Mathematical Methods, Butterworths, London 1982.

31.   Z. Lin, Z. Guan, B. Xu, C. Chen, G. Guo, J. Zhou, J. Xian, L. Cao, L. Wang, M. Li, W. Li, *J of Indus. and Eng. Chem.*2013, **19**, 692-697.

32.   S. Bose, A. R. Bhattacharyya, A. R. Kulkarni and P. Pötschke, *Compos. Sci. Technol*. 2009, **69**, 365-372.

33.   A. V. Poyekar, A. R. Bhattacharyya, R. A. Khare, A. S. Panwar, G. P. Simon, S. Dhar and J.K. Mishra, *Polym. Eng. Sci.* (2014) (in press).

34.   B. Ohlsson, H. Hassander, B. Tornell, *Polymer* 1998, **39**, 6705-6714.

35.   J. Roeder, R.V.B. Oliveira, M.C. Goncalves, V. Soldi, A.T. N Pires, *Polym. Test.* 2002, **21**, 815-821.

36.   I. Y. Phang, J. Ma, J. Shen, T. Liu, W. D. Zhang, *Polym. Int*. 2006, **55**, 71-79.

37.   A. Brosse, S. Tence´-Girault, P.M. Piccione, L. Leibler, *Polymer* 2008, **49**, 4680-4686.

38.   S. Bose, A. R. Bhattacharyya, L. Häußler, P. Pötschke, *Polym. Eng*. Sci. 2009, **49**, 1533-1543.

39.   O.T. Ikkala, R.M. Holsti-Miettinen, J. Seppala, *J Appl Polym Sci* 1993, **49**, 1165-1174.

40.   S. H. Jafari, A. K. Gupta, S. K. Rana, *J Appl. Polym. Sci.* 2000, **75**, 1769-1775.

41.   D. Shi, J. Yin, Z. Ke, Y. Gao, R. K. Li, *J Appl. Polym. Sci*. 2004, **91**, 3742-3755.

42.   M. K. Seo, J. R. Lee, S. J. Park, *Mat. Sci. Eng: A Struct.* 2005, **404**, 79-84.

43.   A. Turner-Jones, J. Aizlewood, D. Beckett, *Makromol. Chem.* 1964, **75**,134-158.

44.   B. D. Cullity, 'Elements of X-ray diffraction, 2nd eds., Addision-Wesley Publication, 1978.

45.   45. G. K. Williamson and W. H. Hall: Acta Metallurgica. 1 (1953) 22.

46.   P. Van Houtte, S. Li, M. Seefeldt, and L. Delannay: *Int. J. Plast.*,2005, 21, 589–624.

47.   L. Delannay, P. J. Jacques, and S. R. Kalidindi: *Int. J. Plast.*, 2006, 22, 1879–98.

48.   M.B. Cortie, Textures and Microstructures, 1997, 29, 155-183.

49.   P. Van Houtte, L. De Buyser, Aeta Metall, mater. 41(1993) 323-336.

50.   I. C. Noyan and J. B. Cohen, Residual Stress Measurement by Diffraction and Interpretation, Springer-Verlag, New york, 1987,117.

51.   B. Verlinden, J. Driver, I. Samajdar, R.D. Doherty, Thermo-Mechanical Processing of Metallic Materials, Pergamon Materials Series, ISBN 978-0-08-044497-0, Elsevier, Amsterdam, 2007.